creative commons
COMMONS DEED

저작자표시-비영리-동일조건변경허락 2.0 대한민국

이용자는 아래의 조건을 따르는 경우에 한하여 자유롭게

- 이 저작물을 복제, 배포, 전송, 전시, 공연 및 방송할 수 있습니다.
- 이차적 저작물을 작성할 수 있습니다.

다음과 같은 조건을 따라야 합니다:

저작자표시. 귀하는 원저작자를 표시하여야 합니다.

비영리. 귀하는 이 저작물을 영리 목적으로 이용할 수 없습니다.

동일조건변경허락. 귀하가 이 저작물을 개작, 변형 또는 가공했을 경우에는, 이 저작물과 동일한 이용허락조건하에서만 배포할 수 있습니다.

- 귀하는, 이 저작물의 재이용이나 배포의 경우, 이 저작물에 적용된 이용허락조건을 명확하게 나타내어야 합니다.
- 저작권자로부터 별도의 허가를 받으면 이러한 조건들은 적용되지 않습니다.

저작권법에 따른 이용자의 권리는 위의 내용에 의하여 영향을 받지 않습니다.

이것은 이용허락규약(Legal Code)을 이해하기 쉽게 요약한 것입니다.

Disclaimer

dCollection

이학석사 학위논문

The Black Hole Mass-Stellar Velocity Dispersion Relation of Narrow Line Seyfert 1 Galaxies

Narrow Line Seyfert 1 은하의 블랙홀 질량과 별속도분산 간의 상관관계 연구

2013 년 8 월

서울대학교 대학원

물리·천문학부 천문학 전공

윤 요 셉

The Black Hole Mass-Stellar Velocity Dispersion Relation of Narrow Line Seyfert 1 Galaxies

A thesis submitted in partial fulfillment of the final requirement for the degree of

Master of Science

Astronomy Program

Department of Physics and Astronomy

Seoul National University

Candidate: **Yosep Yoon**

Supervisor: **Jong-Hak Woo**

June 2013

Abstract

Narrow-Line Seyfert 1 galaxies (NLS1s) are arguably one of the most important AGN subclasses in investigating the origin of the black hole mass−galaxy stellar velocity dispersion ($M_{\rm BH} - \sigma_*$) relation because of their high accretion rates close to the Eddington limit and significantly low black hole masses. Currently, it is still under discussion whether NLS1s offset from the $M_{\rm BH} - \sigma_*$ relation. We identified a sample of 433 NLS1s at relatively low redshift (z $<$ 0.1) from the Sloan Digital Sky Survey Data Release 7 by constraining the full width at half maximum (FWHM) of the broad Balmer line in the range of 800−2200 km s^{-1}. Among them, we measured stellar velocity dispersion of 71 objects which show strong stellar absorption lines, e.g. Mg b triplet ($\sim$5175Å), Fe (5270, 5335Å), and Ca II triplet ($\sim$8500Å). In contrast, the other objects show too weak stellar absorption lines to measure stellar velocity dispersion. Using the sample of 71 objects with σ_* measurements, we investigate whether NLS1s follow the same $M_{\rm BH} - \sigma_*$ relation as normal galaxies and broad-line AGNs. Based on the directly measured σ_*, we find that the NLS1s follow the same $M_{\rm BH} - \sigma_*$ relation as broad-line AGNs and normal galaxies. To test the reliability of the width of narrow lines as a surrogate of σ_*, we compare the directly measured σ_* with the inferred $\sigma_{\rm line}$ from [O III] λ5007 and [S II] $\lambda\lambda$6716, 6731 line width. We find that a good correlation between the σ_* and the width of [S II] whereas a weak correlation for the width of [O III], suggesting that using the width of [O III], as a surrogate for stellar velocity dispersion is unreliable and introduces systematic bias and scatter in the $M_{\rm BH} - \sigma_*$ relation.

Keywords: galaxies: active – galaxies: nuclei – quasars: emission lines

Student Number: 2011 − 23286

Contents

Abstract **i**

1 Introduction **1**

2 Sample selection **5**

2.1 Sample selection 5

2.2 Sample properties 11

3 Analysis **13**

3.1 Multi-component fitting of the emission lines 13

3.2 Black hole mass 27

3.3 Stellar velocity dispersion 33

3.4 Morphology classification 45

4 Result **46**

4.1 The $M_{\rm BH} - \sigma_*$ relation 46

4.2 Comparison between σ_* and narrow emission line widths 49

5 Discussion **52**

6 Summary & Conclusion **55**

Chapter 1

Introduction

Over the past few decades, every galaxy has been thought to having a super massive black hole (SMBH) in the center. Relations between properties of host galaxy and SMBH started to be discovered observationally, e.g., black hole mass−bulge mass relation (Marconi & Hunt 2003; Häring & Rix 2004). Also co−evolution between host galaxy and its black hole was suggested by discovery of black hole mass−stellar velocity dispersion relation, $M_{\rm BH} - \sigma_*$ (Ferrarese & Merritt 2000; Gebhardt et al. 2000; Merritt & Ferrarese 2001). For nearby galaxies, black hole mass can be measured dynamically, but it is not easy for distant galaxies. To overcome this problem, many researchers have used active galactic nuclei (AGNs) which have high luminosity.

AGNs refer to compact regions at the center of galaxies showing energetic phenomena which cannot be attributed to stars and galaxy. AGNs show a very high luminosity over almost all of the electromagnetic spectrum. This extremely high energy of AGNs is considered as a result of accretion by a SMBH at the center of their host galaxies. Thanks to their high luminosity, AGNs have been used to studying distant galaxies and their black holes. AGNs are classified into two types according to their kinds of emission lines. Type 1 AGNs show both broad emission lines with a full width at half-maximum (FWHM) velocity of a few thousand km s^{-1} and narrow emission lines with that of a

few hundreds km s^{-1} while type 2 AGNs show narrow emission lines only.

Osterbrock (1978) suggested an orientation effect to explain the difference between the AGN types with the existence of turbulent, rotating disk just outside and around the accretion disk of the black hole. According to the unification model of AGN (Antonucci 1993), all AGNs have similar physical structure, but the orientation angle makes the various types of AGNs. Broad emission lines and continuum emission are obscured by a dust torus around the accretion disk while narrow emission lines from the outside of the dust torus can be observed. When the unification model was settled down, unusual objects were found emitting "relatively narrow" broad Balmer lines from broad line region (BLR) and strong Fe II emission and positioning the end of $M_{\rm BH} - \sigma_*$ relation. Osterbrock & Pogge (1985) defined these objects as narrow line Seyfert 1 galaxies (NLS1s) by two criteria; one is width of Hβ broad component is less than 2000 km s^{-1} in FWHM, the other is line flux ratio [O III]/Hβ is less than 3. Because of very interesting properties of NLS1s such as low black hole mass, high Eddington ratio and strong Fe II emission, NLS1s are considered relatively young AGNs hosting black holes in a growing phase and became one of the most interesting topics.

The importance of studying the locus of NLS1s on the $M_{\rm BH}-\sigma_*$ plane is emphasized by Mathur et al. (2001) and the $M_{\rm BH}-\sigma_*$ relation of NLS1s has been studied by many researchers. However, previous studies for the $M_{\rm BH}-\sigma_*$ relation of NLS1s using different samples and methods led to controversial results about the locus of the NLS1s on the $M_{\rm BH} - \sigma_*$ relation. In particular, one of the biggest issues is how to determine the σ_* for NLS1s because it is not easy to measure the σ_* due to the contaminations from their luminous AGN continuum and strong Fe II emission. For this reason, after Nelson (2000) suggested the $\rm FWHM_{[OIII]}$ can be used as a surrogate of σ_*, narrow emission lines such as [O III] λ5007, [N II] $\lambda\lambda$6548, 6583 and [S II] $\lambda\lambda$6716, 6731 were used as a surrogate for σ_* in many stuides (Mathur et al. 2001; Wang & Lu 2001; Botte et al. 2004; Grupe & Mathur 2004; Mathur & Grupe 2005a,b; Bian et al. 2006; Zhou et al.

2006; Komossa & Xu 2007; Watson et al. 2007). Among the narrow lines, [O III] λ5007 is most frequently used for the σ_*. When using the width of the [O III] λ5007 narrow emission line as a surrogate for σ_*, some researchers found that the NLS1s lie below the $M_{\rm BH} - \sigma_*$ relation on average with smaller black hole masses for given stellar velocity dispersions compared to normal galaxies (Mathur et al. 2001; Grupe & Mathur 2004; Mathur & Grupe 2005a,b; Bian et al. 2006; Zhou et al. 2006; Watson et al. 2007), while the NLS1s found to be on the $M_{\rm BH} - \sigma_*$ relation in the study of Wang & Lu (2001). Meanwhile, Komossa & Xu (2007) suggested that a careful decomposition of the [O III] λ5007 emission is essential in using the [O III] width due to the complex and asymmetric profile of the [O III]. Komossa et al. (2008) also found a strong correlation between the systematic blueshift of the [O III] and the width of the [O III], which suggests that the systematic blueshift could affect the width of [O III]. They concluded the NLS1s follow the $M_{\rm BH} - \sigma_*$ relation, after removing the asymmetric blue wings and excluding galaxies which have systematic [O III] blueshift which was referred to as "blue outliers". On the other hand, the correlation between the [N II] width and the σ_* was found by Zhou et al. (2006), and Komossa et al. (2008) indicated that the [S II] width can be used as a replacement for the σ_*.

Although considerable research on NLS1s has been conducted by using the width of the narrow emission lines, it is still controversial owing to complexity of narrow lines kinematics and biased in various methods in analyzing the lines. For this reason, more thorough study is necessary. To clarify this ambiguity and to carry out more precise measurements on the $M_{\rm BH}-\sigma_*$ relation of NLS1s, in this study, we focused on direct and accurate measurements of σ_* and black hole mass estimates. We measured σ_* directly by using stellar absorption lines, e.g., Mg b triplet, Fe, Ca II triplet, and black hole mass was carefully estimated with the most recent and various black hole mass estimators. We investigated correlation between various NLS1 properties including emission line width, black hole mass, luminosity, and Eddington ratio, for a sample of 71 NLS1s at z

< 0.1 selected from Sloan Digital Sky Survey Data Release 7 (SDSS DR7) (Abazajian et al. 2009).

We describe the sample selection and the data in section 2, and the fitting procedure and the data analysis in section 3. The results are presented in section 4, followed by discussion in section 5 and summary and conclusions in section 6. Throughout this study, we adopt a cosmology of $H_0 = 70$ km s^{-1} Mpc^{-1}, $\Omega_\Lambda = 0.7$ and $\Omega_\mathrm{m} = 0.3$.

Chapter 2

Sample selection

2.1 Sample selection

NLS1s are defined by following two criteria: (1) width of broad component of the Balmer lines is narrower than 2000 km s^{-1} in FWHM, and (2) line flux ratio [O III] λ5007/Hβ (R5007) is lower than 3 (Osterbrock & Pogge 1985; Goodrich 1989). Additional special features of NLS1s are strong Fe II emission (Osterbrock & Pogge 1985), high Eddington ratio and soft X−ray emission (Leighly 1999; Grupe 2004; McHardy et al. 2006). The strength of Fe II emission is expressed by line flux ratio Fe II $\lambda\lambda$4434−4684/Hβ (R4570). Véron-Cetty et al. (2001) suggested R4570 $>$ 0.5 as a criterion for Fe II emission strength of NLS1s. In this study, we adopted above two main criteria only to select the NLS1s.

To find NLS1s, we used the SDSS DR7 catalogs (Abazajian et al. 2009). The benefit of using the SDSS spectra is to use the very large sample and the proper spectral range. The SDSS spectra covers regions for emission lines e.g., Hα λ6563, Hβ λ4861, [O III] λ5007, [N II] $\lambda\lambda$6548, 6583, [S II] $\lambda\lambda$6716, 6731 and for absorption lines e.g., Mg b region, Ca II region as well. Thanks to the very large sample of SDSS, we could compile large size of sample.

Using the SDSS Query tool (http://casjobs.sdss.org), we selected initial samples by constraining the width of Hβ as 500−2500 km s^{-1} and the equ. width of Hβ as higher than 0, which were taken from the SDSS "SpecLine" class. Because the information provided by the SDSS pipe line process could be incorrect since the pipe line process modeled Hβ emission with single Gaussian without decomposing Hβ into narrow and broad components, we used wider width range than conventional definition in this step. And the equivalent width was used for detecting emission lines. Since we will use the present-day $M_{\rm BH} - \sigma_*$ relation of normal galaxies, we adopted redshift cut z < 0.1. In this step, we found a sample of 4,252 NLS1s.

First of all, we decomposed raw spectrum into featureless AGN continuum, star light and Fe II emission by carrying out multi-component spectral fitting analysis to define NLS1 carefully. An example of multicomponent fitting analysis is illustrated in Figure 2.1 and the fitting procedures are described more in detail in section 3.1. After subtraction of featureless AGN continuum, star light and Fe II emission, we decomposed Hα and Hβ broad and narrow components. As a result, we finalize a sample of 433 NLS1s based on the aforementioned two critieria, i.e., width of broad Balmer line and R5007 < 3. We used broader range of width criterion for Hα broad component ranging 800−2200 km s^{-1}. Because the width criterion for NLS1s was defined conventionally, and fitting results could be changed with depending on various fitting methods. Other more characteristics of NLS1 such as weakness of [O III] emission, strong Fe II emission were used to identify NLS1s, using our width criterion is reliable. The width distribution of the Balmer lines of our sample is shown in Figure 2.2. In following section, we will discuss the sample properties in detail. We finalized 71 objects which could be measured stellar velocity dispersion except rest 362 objects showing too weak stellar absorption lines to measure σ_*. The process to measure σ_* is explained in section 3.3. Total list of NLS1s is shown in Table.2.1. We listed name of object in the column (2), redshift in the column (3).

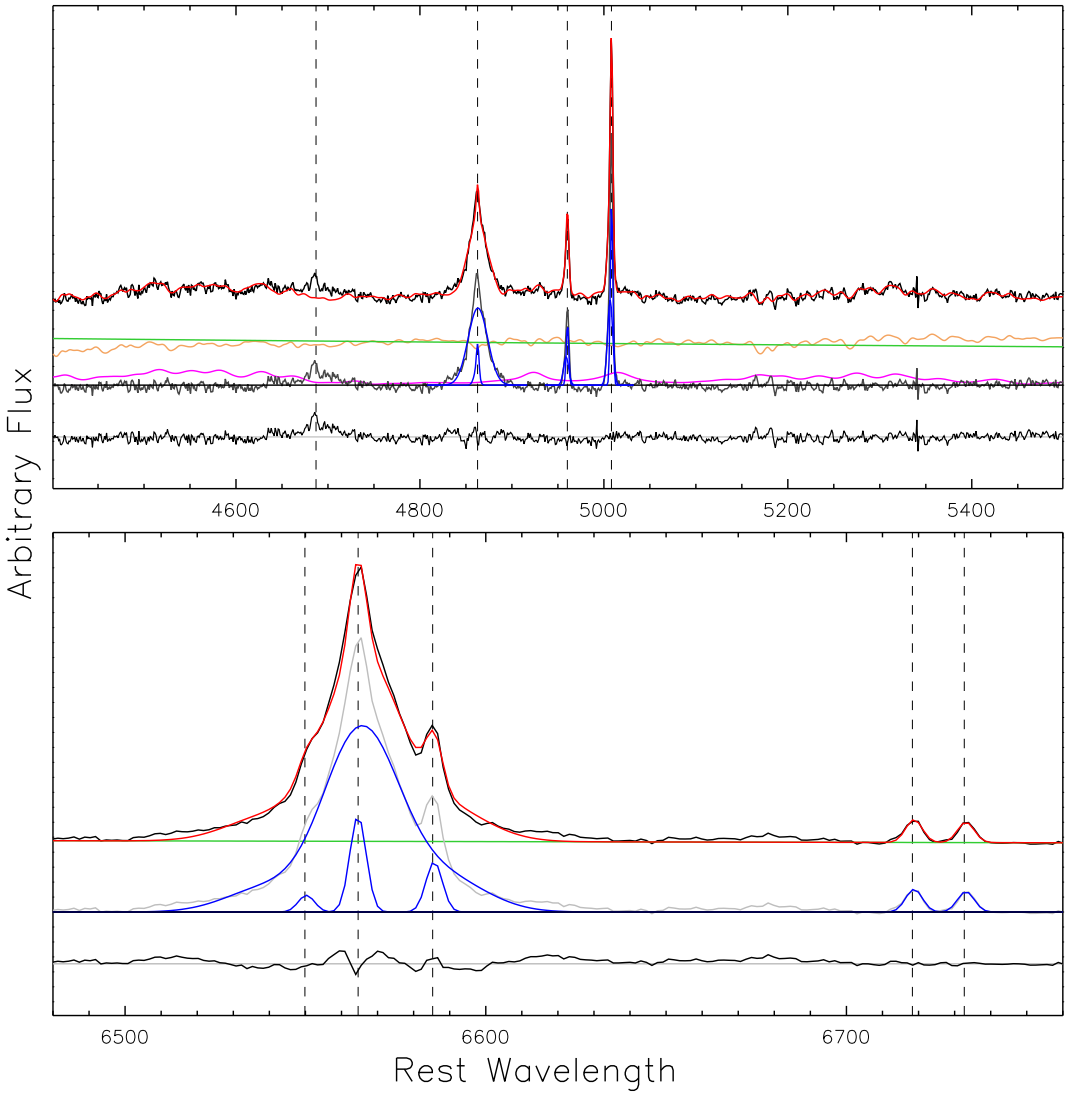

Figure 2.1: An example of decomposition precess for the Hβ and Hα regions. In both panels, raw spectra converted to rest frame (black) and the sum of all models (red) are presented in the upper side, and models for emission lines (blue) are shown in the lower side. In the Hβ region (top panel), the best-fit power-law continuum (green), the host galaxy star light model (orange), and the Fe II model (magenta) is presented. The residual is arbitrarily moved downward to clarify in both panels.

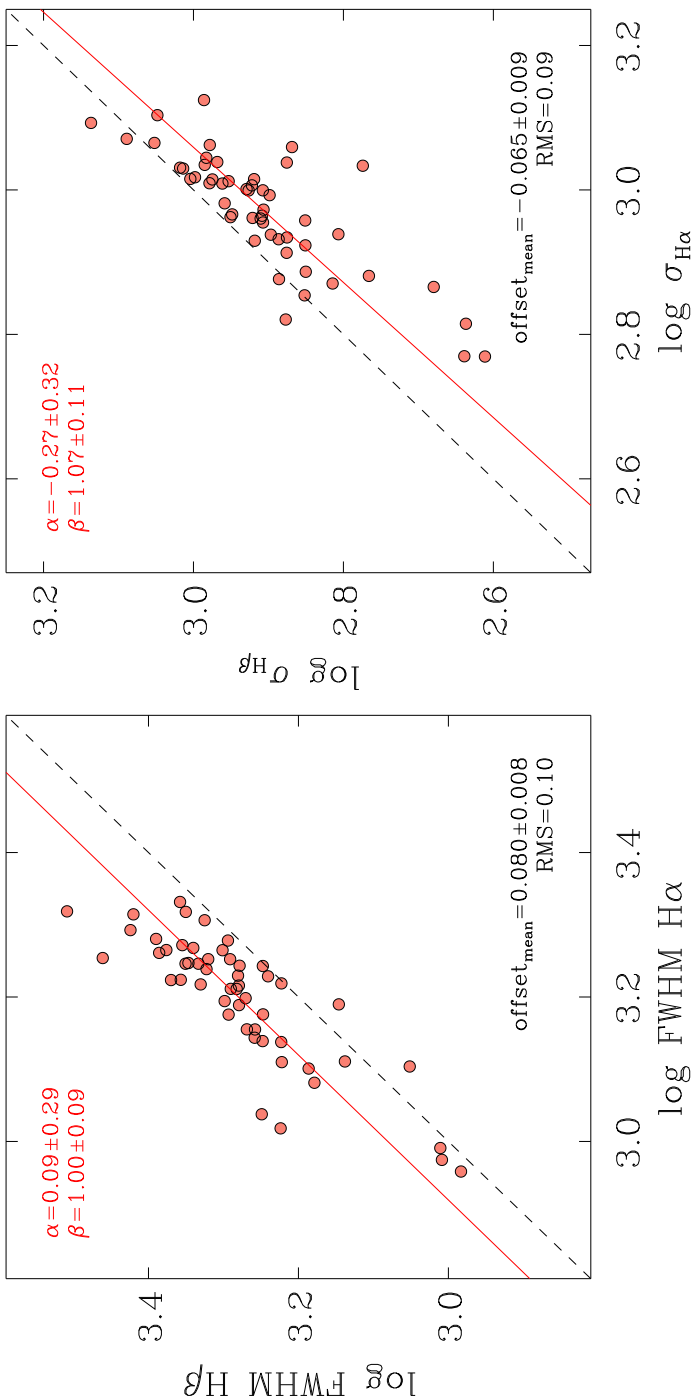

Figure 2.2: Comparison between broad component of Hα and Hβ for FWHM (left) and σ (right). Only high quality targets (S/N of Hb > 20) are expressed. For the Hβmeasurements, Hβ is modeled with single Gaussian, $\mathrm{FWHM}_{\mathrm{H}\beta}$ and $\sigma_{\mathrm{H}\beta}$ represent same result with a relation of $\mathrm{FWHM}_{\mathrm{H}\beta} = 2.35\ \sigma_{\mathrm{H}\beta}$.

Table 2.1: The list of NLS1s

No. (1)	Objectname. (2)	Redshift (3)	$\log M_{\rm BH}$ (this study)(4)	$\log M_{\rm BH}$ (GH05)(5)	$\log M_{\rm BH}$ (McGill+08)(6)	$\log M_{\rm BH}$ (Park+12)(7)	$\sigma_{\rm Mgb}$ (8)	$\sigma_{\rm noMgb}$ (9)	$\sigma_{\rm CaT}$ (10)	type (11)	inclination (12)
1	J010409.16 + 000843.7	0.071	6.61	6.41	6.48	6.09	67 ± 12	76 ± 18	84 ± 25	late	edge-on
2	J030417.78 + 002827.3	0.045	6.68	6.36	6.54	6.25	71 ± 12	73 ± 13	66 ± 12	late	face-on
3	J073106.86 + 392644.6	0.049	6.44	6.14	6.28	5.86	61 ± 11	57 ± 6	62 ± 7	late	face-on
4	J073714.27 + 292634.2	0.080	6.97	6.62	6.84	6.55	93 ± 15	98 ± 19		late	face-on
5	J080253.18 + 130559.6	0.095	7.33	7.12	7.25	7.00	92 ± 19	114 ± 23		early	
6	J080538.22 + 244214.8	0.099	6.87	6.57	6.76	6.34	98 ± 24	113 ± 32		early	
7	J080629.8 + 241955.6	0.042	6.27	5.87	6.08	6.14	$71 \pm 5^*$	71 ± 15	70 ± 15	late	face-on
8	J080801.74 + 381935.3	0.041	6.65	6.37	6.46	6.19	85 ± 15	82 ± 18		late	face-on
9	J081718.56 + 520147.7	0.039	6.67	6.36	6.51	6.35	66 ± 11	67 ± 12	89 ± 28	early	
10	J082007.8 + 372839.6	0.082	7.04	6.64	6.90	6.71	148 ± 20	167 ± 28		late	intermediate
11	J082912.67 + 500652.3	0.043	6.43	6.09	6.30	5.81	$60 \pm 2^*$	75 ± 18	89 ± 21	early	
12	J083202.15 + 461425.7	0.046	7.00	6.64	6.87	6.57	109 ± 7	124 ± 10	100 ± 21	late	face-on
13	J083741.94 + 263344.1	0.076	6.98	6.68	6.84	6.58	101 ± 18	89 ± 18		early	
14	J083949.64 + 484701.4	0.039	6.96	6.63	6.84	6.58	92 ± 11	100 ± 10	113 ± 18	late	intermediate
15	J084927.37 + 324852.7	0.064	7.26	6.97	7.14	6.97	134 ± 14	130 ± 18	140 ± 42	late	intermediate
16	J085504.17 + 525248.3	0.090	7.09	6.83	7.00	6.57	109 ± 18	121 ± 25		late	intermediate
17	J092438.88 + 560746.9	0.025	6.69	6.44	6.52	5.89	130 ± 6	141 ± 8	94 ± 17	late	edge-on
18	J093638.69 + 132529.6	0.091	6.97	6.77	6.83	6.99	83 ± 15	80 ± 16		late	face-on
19	J094153.41 + 163621	0.051	6.83	6.66	6.66	6.14	97 ± 16	90 ± 19		early	
20	J094529.36 + 093610.4	0.013	6.49	6.22	6.28	6.06	$76 \pm 2^*$	64 ± 9	62 ± 10	late	intermediate
21	J095151.82 + 060143.7	0.093	6.53	6.12	6.36	6.06	$76 \pm 6^*$	97 ± 25		early	
22	J095848.66 + 025243.2	0.079	6.84	6.52	6.68	6.36	101 ± 13	96 ± 15		early	
23	J100854.93 + 373929.9	0.054	7.25	7.01	7.17	6.89	97 ± 11	134 ± 16	143 ± 25	early	
24	J102532.08 + 102504	0.046	6.88	6.57	6.73	6.34	93 ± 10	121 ± 15	71 ± 17	early	
25	J103103.53 + 462616.8	0.093	7.21	6.99	7.12	6.83	177 ± 18	195 ± 25		late	edge-on
26	J103751.82 + 334850.1	0.051	6.82	6.47	6.63	6.28	91 ± 14	80 ± 17	86 ± 20	late	face-on
27	J104153.59 + 031500.6	0.094	7.23	6.94	7.12	6.90	158 ± 31	139 ± 42		late	intermediate
28	J105600.4 + 165626.1	0.085	7.00	6.76	6.87	6.55	123 ± 21	105 ± 21		late	intermediate
29	J110016.03 + 461615.2	0.032	6.59	6.38	6.42	6.06	55 ± 4	57 ± 6	76 ± 15	late	face-on
30	J111031.61 + 022043.2	0.080	6.59	6.24	6.46	6.24	$77 \pm 3^*$	69 ± 13		early	
31	J111253.12 + 314807.3	0.076	7.33	6.97	7.23	7.01	72 ± 14	73 ± 16		early	
32	J111407.35 − 000030.9	0.073	6.96	6.58	6.83	6.54	121 ± 17	103 ± 17	79 ± 23	late	face-on

Col. (1): Number. Col. (2): Object name given by its SDSS coordinate designation. Col. (3): Redshift. Col. (4): $M_{\rm BH}$ in this study by using $\sigma_{\rm H\alpha}$ and $L_{\rm H\alpha}$ measurements. Col. (5): $M_{\rm BH}$ determined by the equation from Greene & Ho (2005) with FWHM$_{\rm H\alpha}$ and $L_{\rm H\alpha}$. Col. (6): $M_{\rm BH}$ determined by the equation from McGill et al. (2008) with $\sigma_{\rm H\alpha}$ and $L_{\rm H\alpha}$. Col. (7): $M_{\rm BH}$ determined by the equation from Park et al. (2012) with $\sigma_{\rm H\beta}$ and AGN continuum luminosity. Col. (8)−(10): Stellar velocity dispersion measured in Mg *b* region with Mg *b* region and without Mg *b*, and in Ca II region. The σ_* measurements from Xiao et al. (2011) are expressed by *. Col. (11): Classification of galaxy type. Col. (12): Classification of inclination angle of galaxy.

Table 2.2: The list of NLS1s

No. (1)	Objectname. (2)	Redshift (3)	$\log M_{\rm BH}$ (this study)(4)	$\log M_{\rm BH}$ (GH05)(5)	$\log M_{\rm BH}$ (McGill+08)(6)	$\log M_{\rm BH}$ (Park+12)(7)	$\sigma_{\rm Mgb}$ (8)	$\sigma_{\rm noMgb}$ (9)	$\sigma_{\rm CaT}$ (10)	type (11)	inclination (12)
33	$J112229.65+214815.5$	0.061	7.01	6.71	6.87	6.60	120 ± 9	11611	140 ± 19	late	face-on
34	$J112502.62+563640.7$	0.100	7.32	7.00	7.21	6.91	183 ± 18	180 ± 24		late	edge-on
35	$J112526.51+022039$	0.049	6.69	6.24	6.52	6.17	100 ± 17	98 ± 16		early	
36	$J112545.35+240823.9$	0.024	6.13	5.73	5.90	5.34	64 ± 7	66 ± 9	72 ± 15	late	face-on
37	$J113101.1+134539.6$	0.092	7.24	6.97	7.14	6.72	166 ± 21	225 ± 25		late	edge-on
38	$J113111.94+100231.3$	0.074	6.88	6.66	6.73	6.69	129 ± 21	154 ± 29		late	edge-on
39	$J113913.91+335551.1$	0.032	6.85	6.55	6.74	6.32	100 ± 15	130 ± 23		late	face-on
40	$J115333.22+095408.3$	0.069	7.08	6.88	6.96	6.62	113 ± 12	108 ± 16		early	
41	$J120012.47+183542.9$	0.067	6.73	6.39	6.56	6.01	111 ± 16	98 ± 17		late	face-on
42	$J121157.48+055801.1$	0.068	7.15	7.00	7.05	6.59	120 ± 24	122 ± 18		late	face-on
43	$J122307.79+192337.1$	0.076	7.02	6.70	6.88	6.66	113 ± 14	122 ± 14		late	intermediate
44	$J122342.8+581446.1$	0.015	6.20	5.67	5.99	5.80	$45 \pm 2^{*}$	57 ± 6	64 ± 11	early	
45	$J123651.17+453904.1$	0.030	6.76	6.54	6.62	6.29	81 ± 13	85 ± 12	98 ± 19	late	face-on
46	$J123932.59+342221.3$	0.084	6.95	6.69	6.83	6.79	75 ± 10	83 ± 13		early	
47	$J124319.98+025256.1$	0.087	6.86	6.56	6.76	6.57	103 ± 14	104 ± 16		early	
48	$J130456.95+395529.7$	0.028	6.52	6.09	6.30	6.03	70 ± 8	70 ± 10	93 ± 19	late	face-on
49	$J131142.56+331612.8$	0.079	7.06	6.82	6.92	6.43	90 ± 15	103 ± 20		late	face-on
50	$J131305.8+012755.9$	0.030	6.63	6.35	6.45	6.02	99 ± 7	93 ± 9	79 ± 15	late	face-on
51	$J131905.95+310852.8$	0.032	7.02	6.62	6.83	6.56	124 ± 8	121 ± 11	129 ± 34	late	intermediate
52	$J134240.08+022524.3$	0.074	6.81	6.56	6.64	6.38	103 ± 15	80 ± 16		early	
53	$J134401.9+255628.3$	0.062	7.06	6.62	6.92	6.29	129 ± 13	136 ± 15	124 ± 26	late	intermediate
54	$J140659.58+231738.7$	0.060	6.73	6.20	6.53	6.06	88 ± 12	88 ± 15	65 ± 13	early	
55	$J141434.52+293428.2$	0.076	6.77	6.41	6.63	6.58	72 ± 15	68 ± 15		early	
56	$J143658.68+164513.6$	0.072	6.55	6.26	6.37	6.06	66 ± 10	72 ± 16		early	
57	$J143708.46+074013.6$	0.087	6.92	6.75	6.77	6.28	99 ± 16	82 ± 16		early	
58	$J151356.89+481012.1$	0.079	6.83	6.54	6.72	6.32	122 ± 20	135 ± 27		late	intermediate
59	$J152209.55+451124.1$	0.066	6.87	6.72	6.73	6.25	102 ± 21	124 ± 18		late	intermediate
60	$J152324.42+551855.3$	0.039	6.91	6.52	6.74	6.15	119 ± 9	115 ± 12	108 ± 30	late	edge-on
61	$J152940.58+302909.3$	0.036	7.16	6.88	7.05	6.83	92 ± 9	98 ± 12	77 ± 13	late	face-on
62	$J155640.9+121718$	0.036	6.93	6.64	6.76	6.43	138 ± 10	143 ± 15	123 ± 14	early	
63	$J160746.01+345048.9$	0.054	6.78	6.58	6.66	6.49	61 ± 8	82 ± 17	96 ± 22	early	
64	$J161527.67+403153.7$	0.084	6.85	6.60	6.71	6.60	125 ± 24	120 ± 22		early	
65	$J161809.37+361957.8$	0.034	6.39	5.97	6.24	5.75	78 ± 11	70 ± 11		early	
66	$J161951.31+405847.2$	0.038	6.94	6.62	6.79	6.37	87 ± 14	140 ± 18	101 ± 20	late	edge-on
67	$J162930.01+420703.2$	0.072	6.82	6.53	6.68	6.47	101 ± 20	76 ± 16		late	face-on
68	$J163159.59+243740.2$	0.044	6.43	5.94	6.28	5.80	70 ± 10	65 ± 13	74 ± 18	early	
69	$J163501.45+305412.1$	0.054	6.94	6.47	6.83	6.30	133 ± 16	137 ± 22	110 ± 28	late	edge-on
70	$J210226.54+000702.3$	0.052	6.46	6.16	6.27	6.28	85 ± 19	81 ± 18	73 ± 17	late	face-on
71	$J210533.43+002829.2$	0.054	6.73	6.37	6.58	6.39	68 ± 13	79 ± 14	89 ± 23	early	

Table 2.1 continued

2.2 Sample properties

Two striking features of NLS1s are weak [O III] emission (Osterbrock & Pogge 1985; Goodrich 1989) and strong Fe II emission (Osterbrock & Pogge 1985; Véron-Cetty et al. 2001). These two properties, as expressed by R5007 and R4570 described in section 2.1, are used to distinguish NLS1 from other galaxies. Including R5007 index to define NLS1 is not always used in the previous studies of NLS1s. For example, Williams et al. (2002) used the R5007 for identifying NLS1s while Zhou et al. (2006); Komossa & Xu (2007) only used the criterion of width Balmer lines. In our study, we used the criterion R5007 (flux [O III] / flux Hβ) < 3 to conservatively define NLS1s. All of our sample satisfy this condition.

The index of Fe II strength, R4570, is expressed by line flux ratio of Fe II $\lambda\lambda$4434$-$4684 over Hβ emission. One unclear issue of R4570 is whether Hβ broad component or Hβ total flux should be used in calculating R4570. For exmaplem in Zhou et al. (2006), the flux of Hβ broad component is used, resulting that the mean of R4570 is 0.82. Meanwhile, Xu et al. (2012) adopted Hβ total flux for R4570, and the mean R4570 of their NLS1s is 0.7 with a range of 0.1$-$2.7. The mean of R4570 of our sample is 1.27 when the Hβ broad component is used, and it is 1.02 when the total Hβ profile is used. In the case of general AGN population, $\sim$5% of AGNs have R4570 (Hβ BC) > 1 (Lawrence et al. 1988). In contrast, 59.2% of our sample have R4570 > 1, indicating our sample is consistent with NLS1s . The distribution of R5007 and R4570 for our NLS1s sample are shown in Figure 2.3.

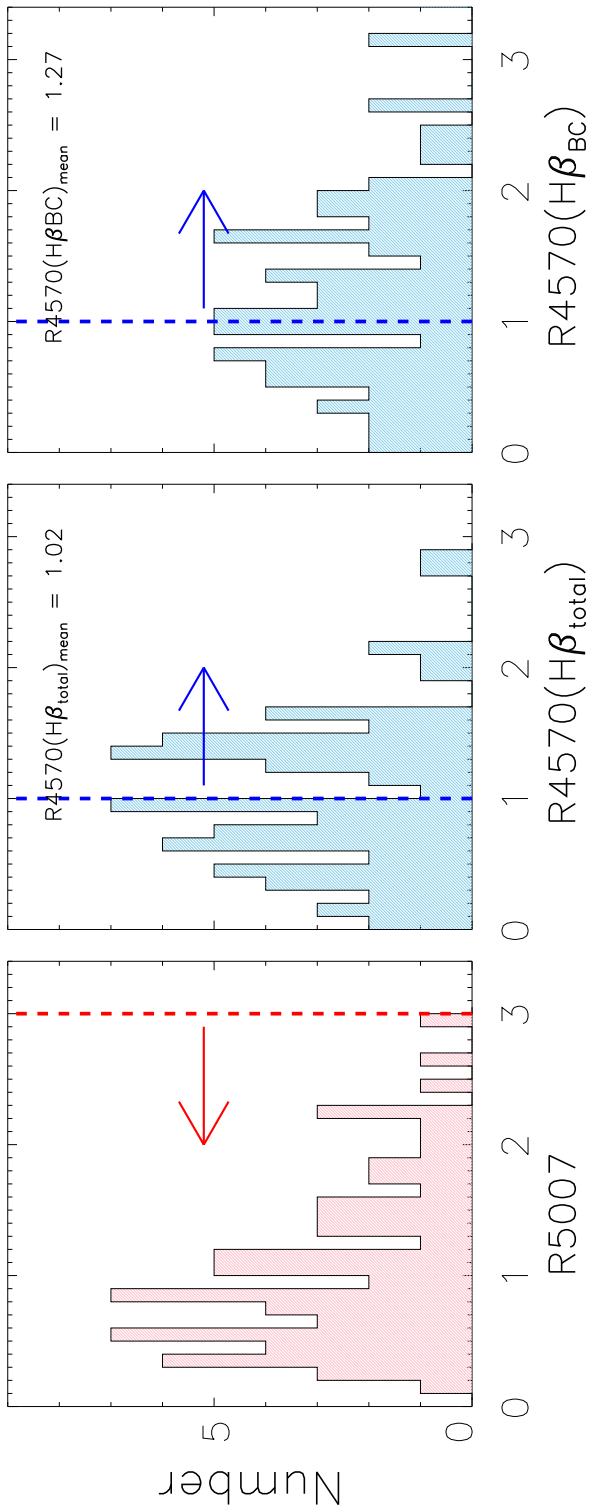

Figure 2.3: Distribution of R5007 and R4570 for our NLS1s. All of our NLS1 sample satisfy the condition of R5007 < 3. The fraction of R4570 (Hβ BC) > 1 is 59.1% (middle), and the fraction of R4570 (Hβ total) > 1 is 45.1% (right). These fractions are much higher value than its of normal AGNs.

Chapter 3

Analysis

In order to measure the $M_{\rm BH} - \sigma_*$ relation of NLS1s, we measure black hole mass and stellar velocity dispersion. In this section, we present multi-components spectral fitting methods (Section 3.1), and analysis to determine black hole mass (Section 3.2), and to measure the stellar velocity dispersion (Section 3.3). In addition, we describe the morphology classification process for the host galaxies. Since we are able to measure the stellar velocity dispersions of 71 objects, we present the results for these objects although we performed the fitting procedure for the 433 NLS1s in the total sample.

3.1 Multi-component fitting of the emission lines

We performed multi-components spectral fitting analysis in two separate spectral ranges: Hβ region (4400$-$5580Å) and Hα region (6500$-$6800Å). Detailed fitting methods for these two region are described below.

For the Hβ region, we followed the procedure given by (Woo et al. 2006; McGill et al. 2008; Park et al. 2012). After converting all spectra to the rest frame, we modeled the observed spectra with three components, i.e., featureless AGN continuum, host-galaxy starlight, and Fe II emission blends by respectively using single power law continuum, a stellar template from Bruzual & Charlot (2003), and an Fe II template from (Boroson &

Green 1992). The best continuum model was determined in the regions 4430–4600Å and 5080−5550Å where Fe II emission dominates. We simultaneously conducted fitting for all 3 components, using the nonlinear Levenberg-Marquardt least-squares fitting routine *mpfit* (Markwardt 2009) in IDL. A set of stellar templates of INDO−US stellar library, which includes spectra of four K giants, three G giants, an F2 and an A0 giants, is used (Valdes et al. 2004). After subtracting the featureless AGN continuum and host-galaxy starlight from the raw spectra, emission lines fitting for Hβ, [O III] λ4959 and [O III] λ5007 was carried out for this region. Komossa & Xu (2007) found that [O III] λ5007 shows often complex profile such as velocity shift of [O III] core and asymmetry. To resolve this [O III] complexity, decomposing [O III] into a narrow core and a broad base. We modeled [O III] by dividing into two groups according to [O III] spectral complexity same as the method used in Komossa & Xu (2007). First, if [O III] has the broad base which tends to show blue−asymmetric (blue wing), the [O III] was decomposed by double Gaussian for a narrow core and a broad base. The broad base component was excluded, and the width was measured with only the narrow core. However, if [O III] is symmetrical or of low S/N, the [O III] is fitted with a single Gaussian. After modeling the [O III] λ5007, it was used to model [O III] λ4959 and Hβ narrow component by assuming same widths between narrow emission lines. The height of [O III] λ4959 was scaled by 1/3 of [O III] λ5007, but the height of the Hβ narrow component was set as free parameter. Next, we fitted Hβ broad component with single Gaussian. Hβ emission are often asymmetric, thus using Gauss-Hermite series is more suitable. We, however, decided to use single Gaussian fitting due to because of low S/N of Hβ emission. The Hβ emission line of all NLS1s in our sample is not blended with He II λ4686, thus subtracting He II was not considered.

For the Hα region, in contrast, we did not subtract Fe II emission because of its weakness in this range. After converting all spectra to the rest frame same as the Hβ region, we begin the fitting process with continuum subtraction. Two regions 6400–6460Å and

6740−6800Å were used to determine the best continuum model where no other emission and absorption lines are. After subtracting the continuum from converted spectra, first we modeled [S II] λ6716 and [S II] λ6731 with each single Gaussian because [S II] doublet is not blended by other emission lines and it can be decompose easily and precisely. After fitting [S II] doublet, we performed Hα+[N II] blended region fitting by dividing into two groups according to S/N of [S II]. For high quality targets (S/N of [S II] $>$ 25), we brought the width of [S II] to the widths of Hα narrow component and [N II] doublet on the assumption that line widths of narrow lines are similar to each other. For the other low quality targets, Hα narrow component and [N II] doublet were fitted with same the width which is not same as [S II] width. The flux of [N II] λ6548 was scaled by 1/3 of that of [N II] λ6583. For Hα broad component, Gauss-Hermitian fitting was used to model complex Hα profile (McGill et al. 2008). All fitting results for those two regions are shown in Figure 3.1−3.9.

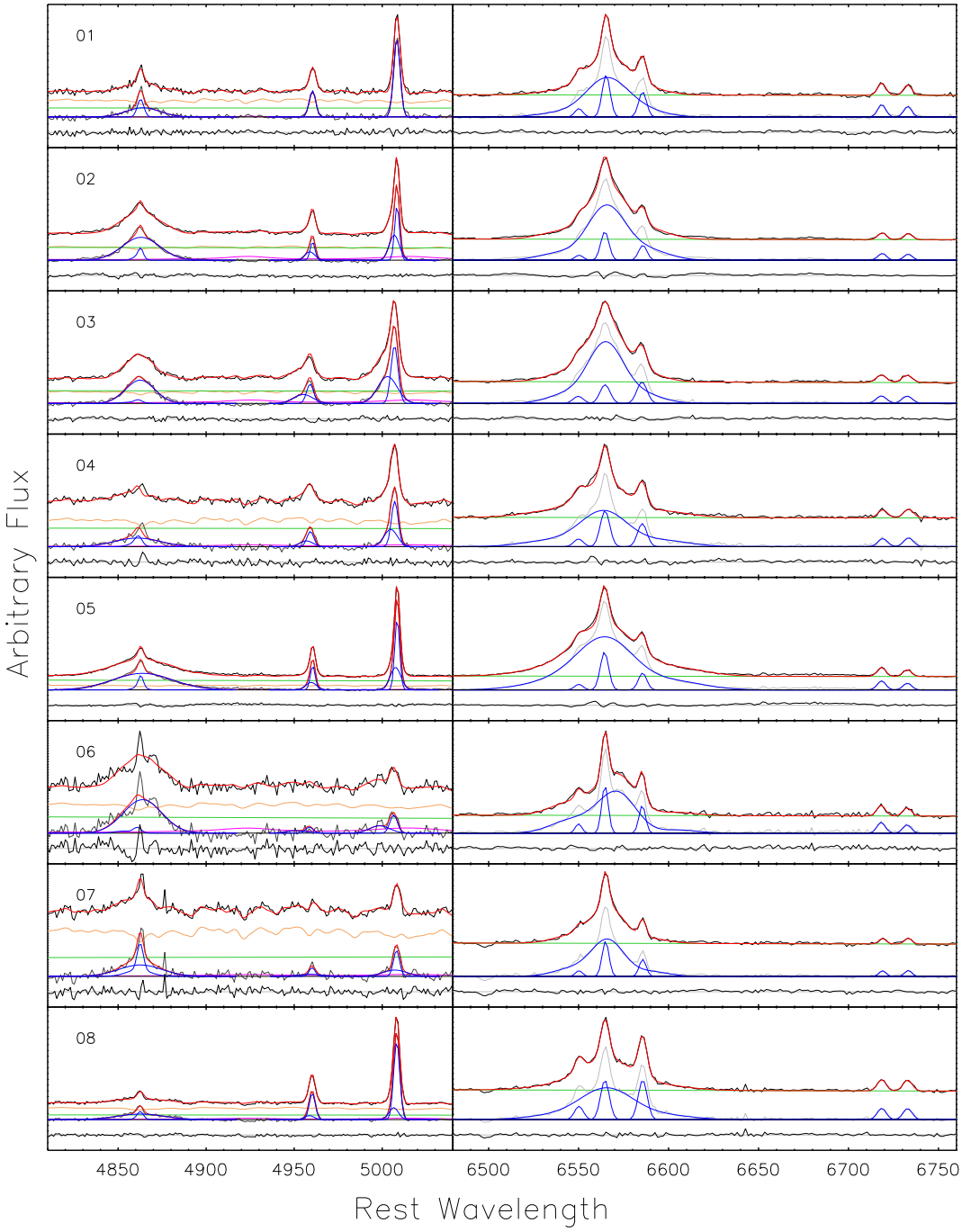

Figure 3.1: The spectral fitting results of all 71 NLS1s. Left and right panels show fitting results of Hβ region and Hα region, respectively. The results are illustrated as follows: raw spectra (black), total model fit (red), emission line fits (blue), and for the Hβ region,best-fit power-law continuum (green), host galaxy star light model (orange), Fe II model (magenta). The residual is arbitrarily moved downward to clarify.

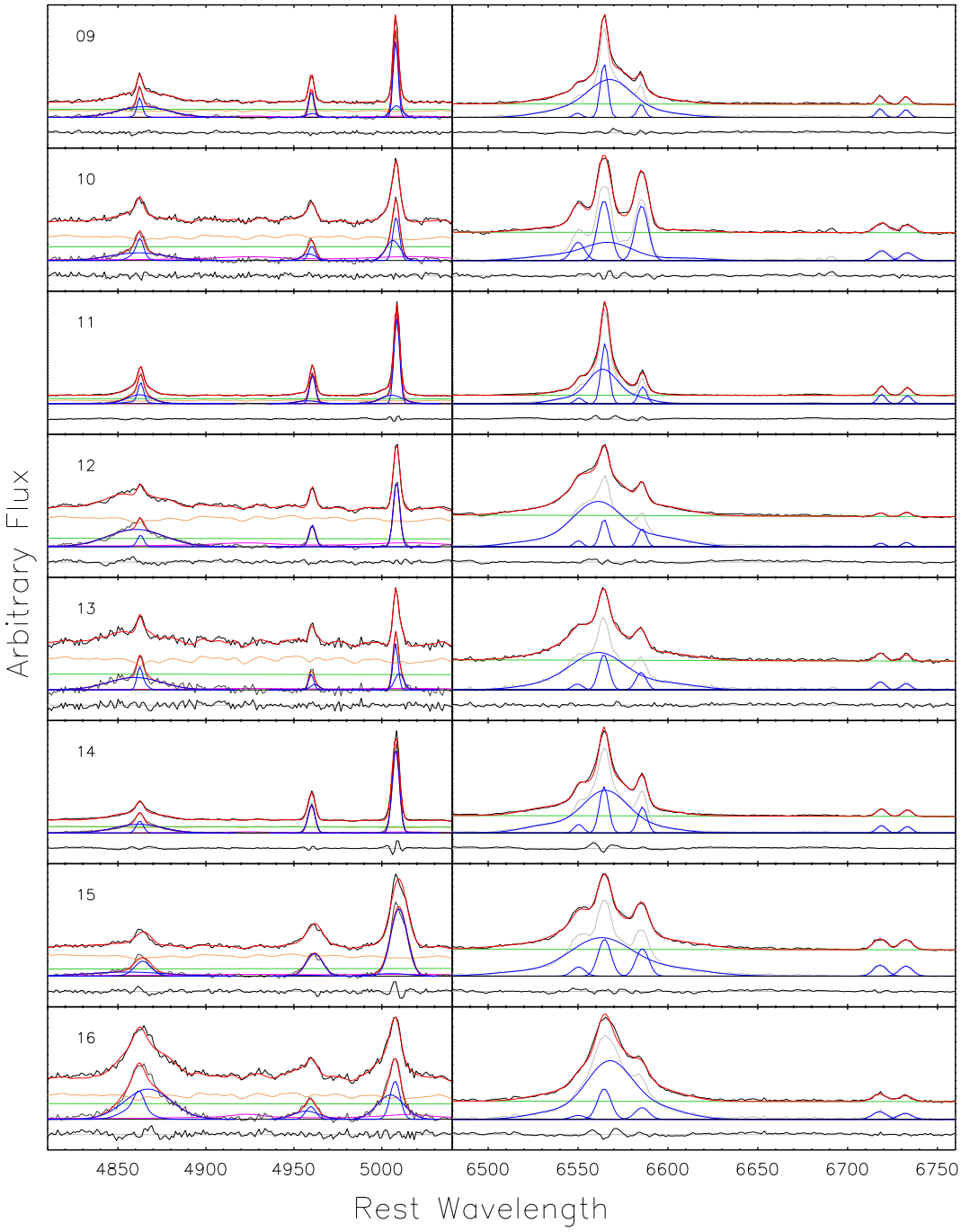

Figure 3.2: Continued

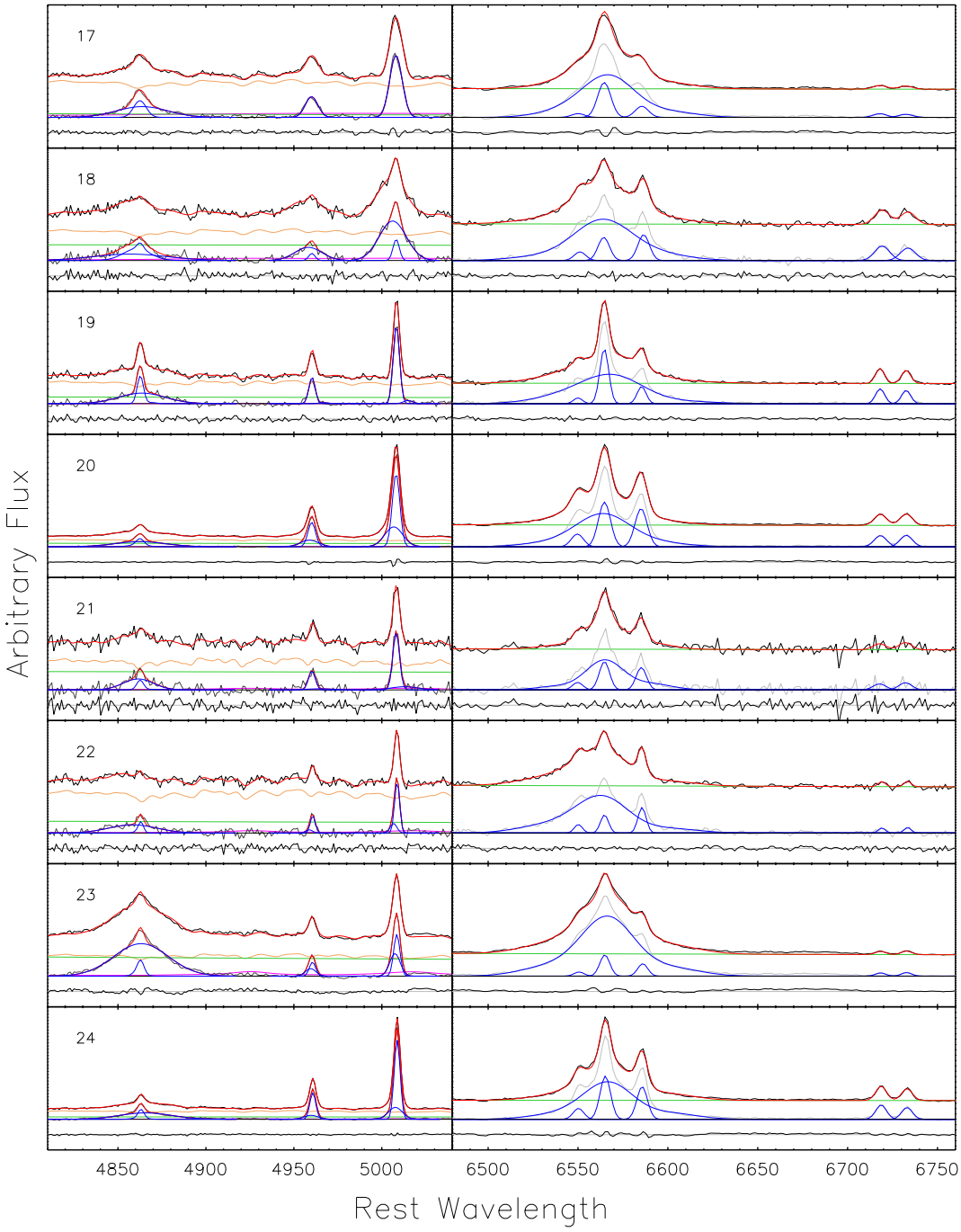

Figure 3.3: Continued

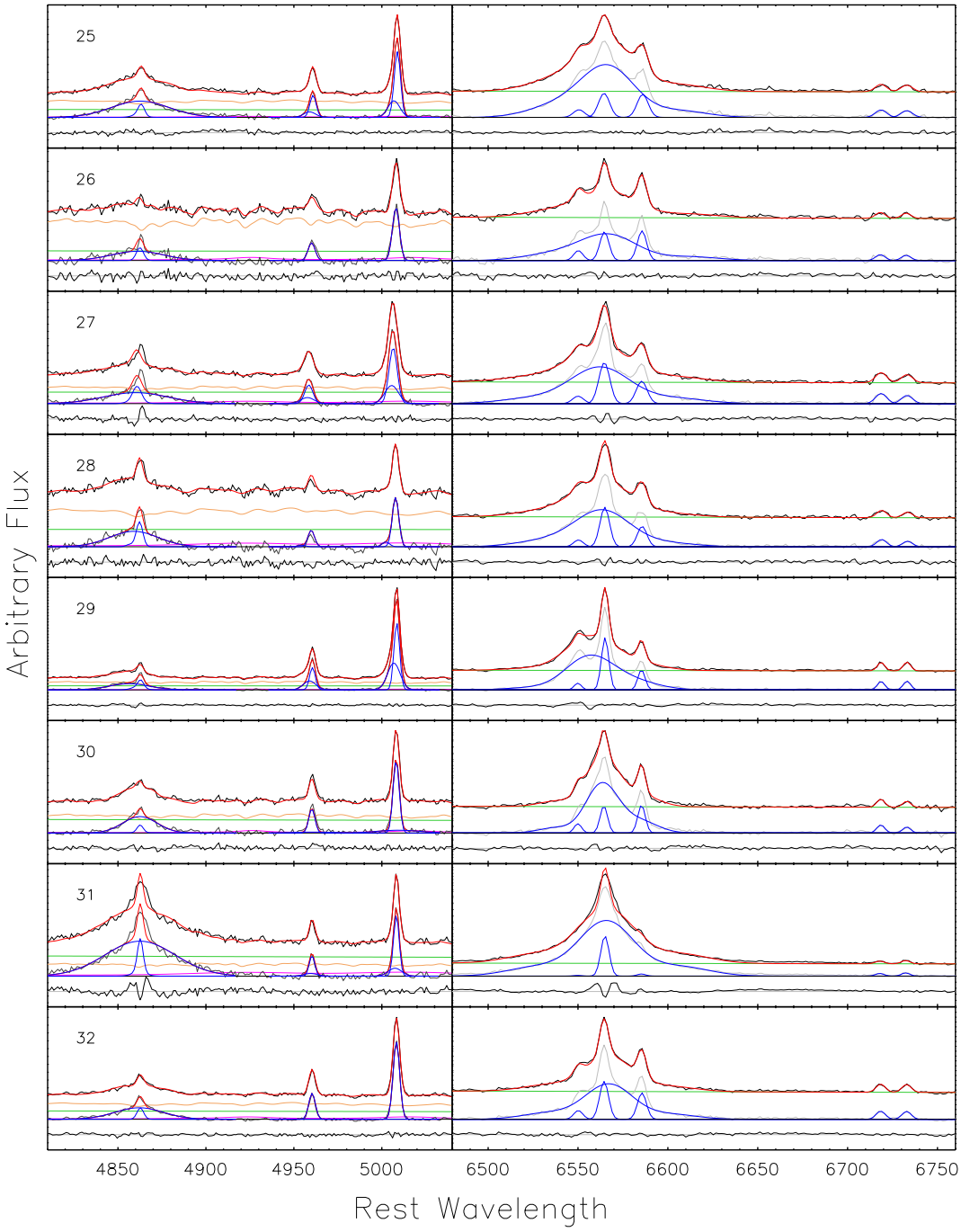

Figure 3.4: Continued

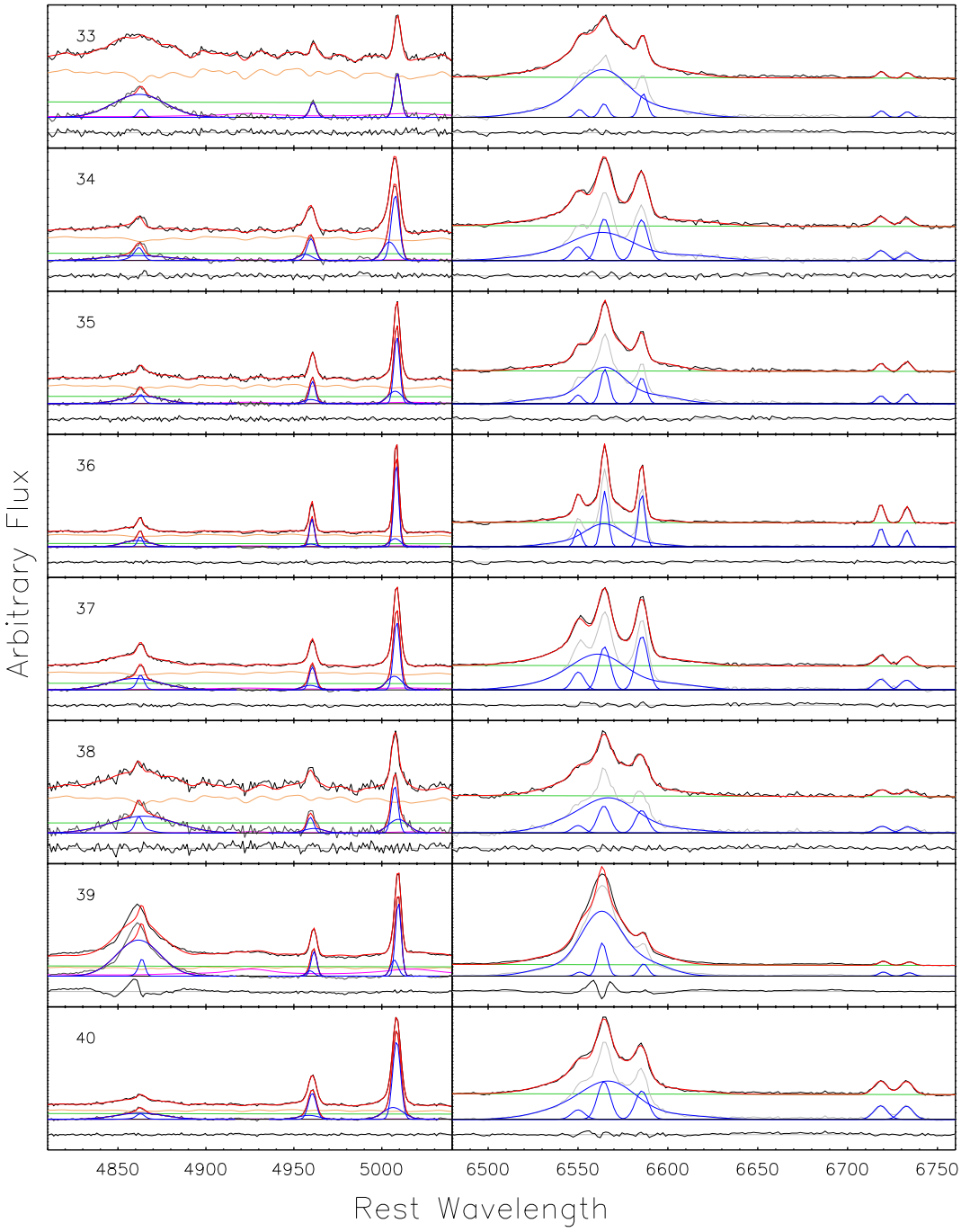

Figure 3.5: Continued

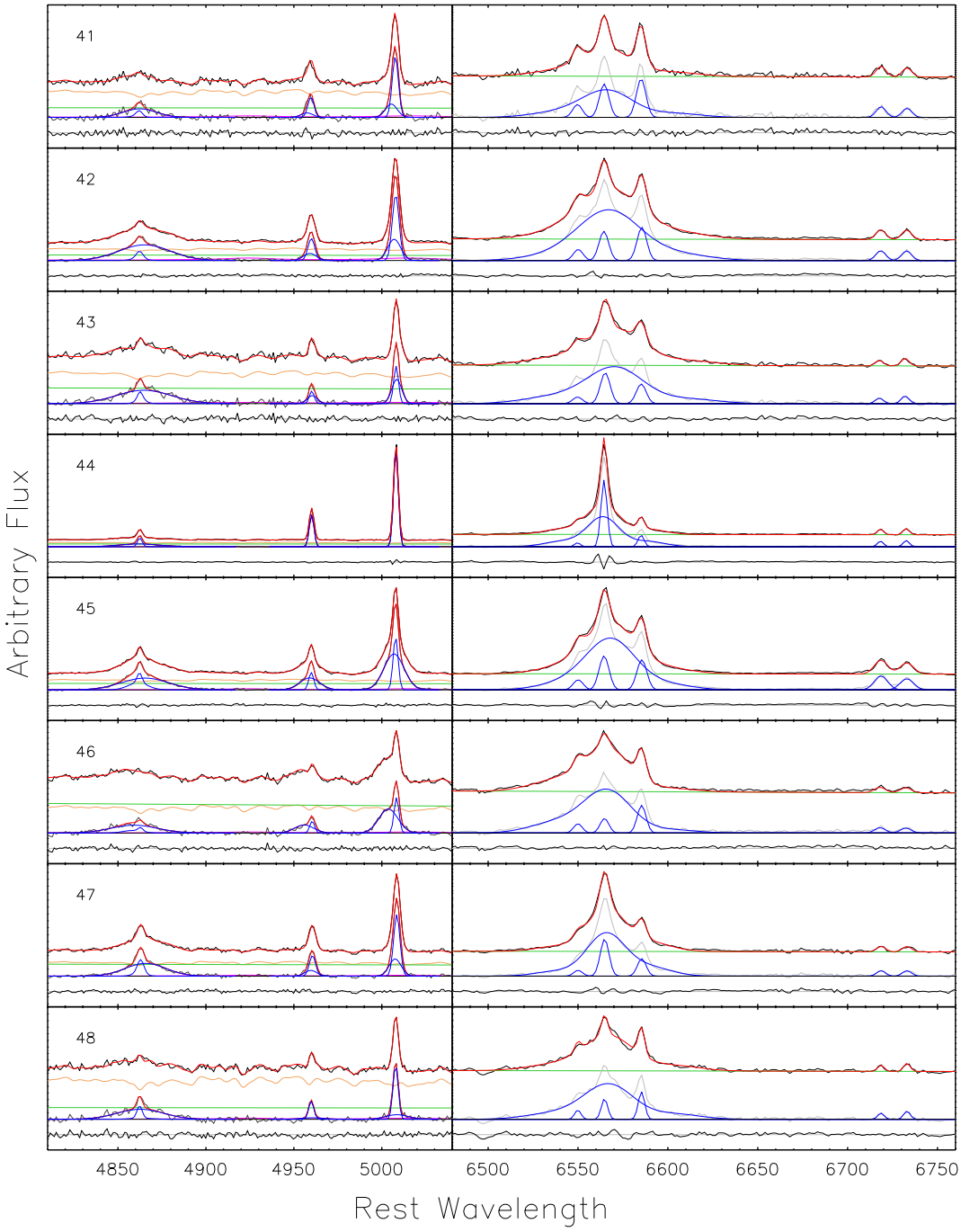

Figure 3.6: Continued

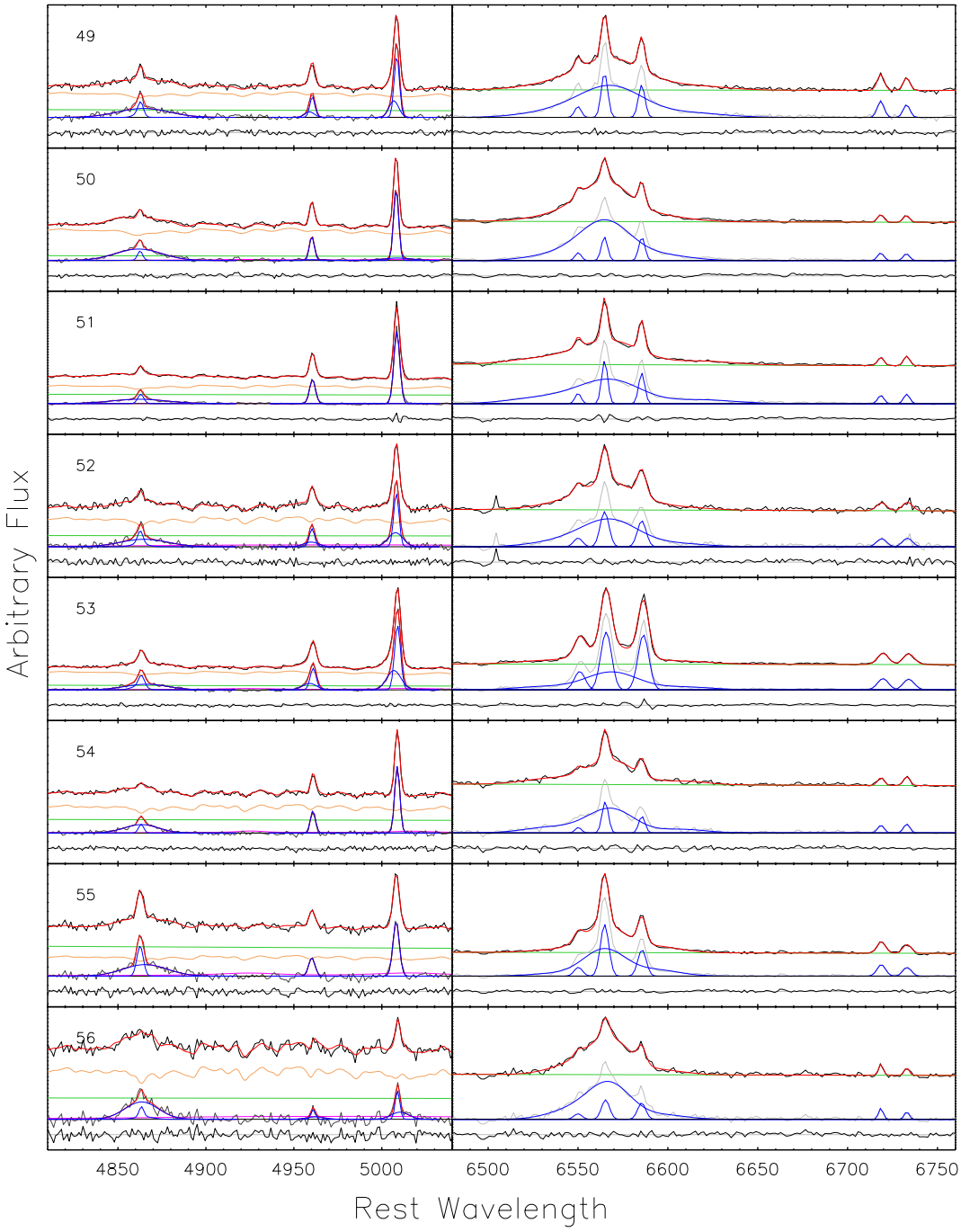

Figure 3.7: Continued

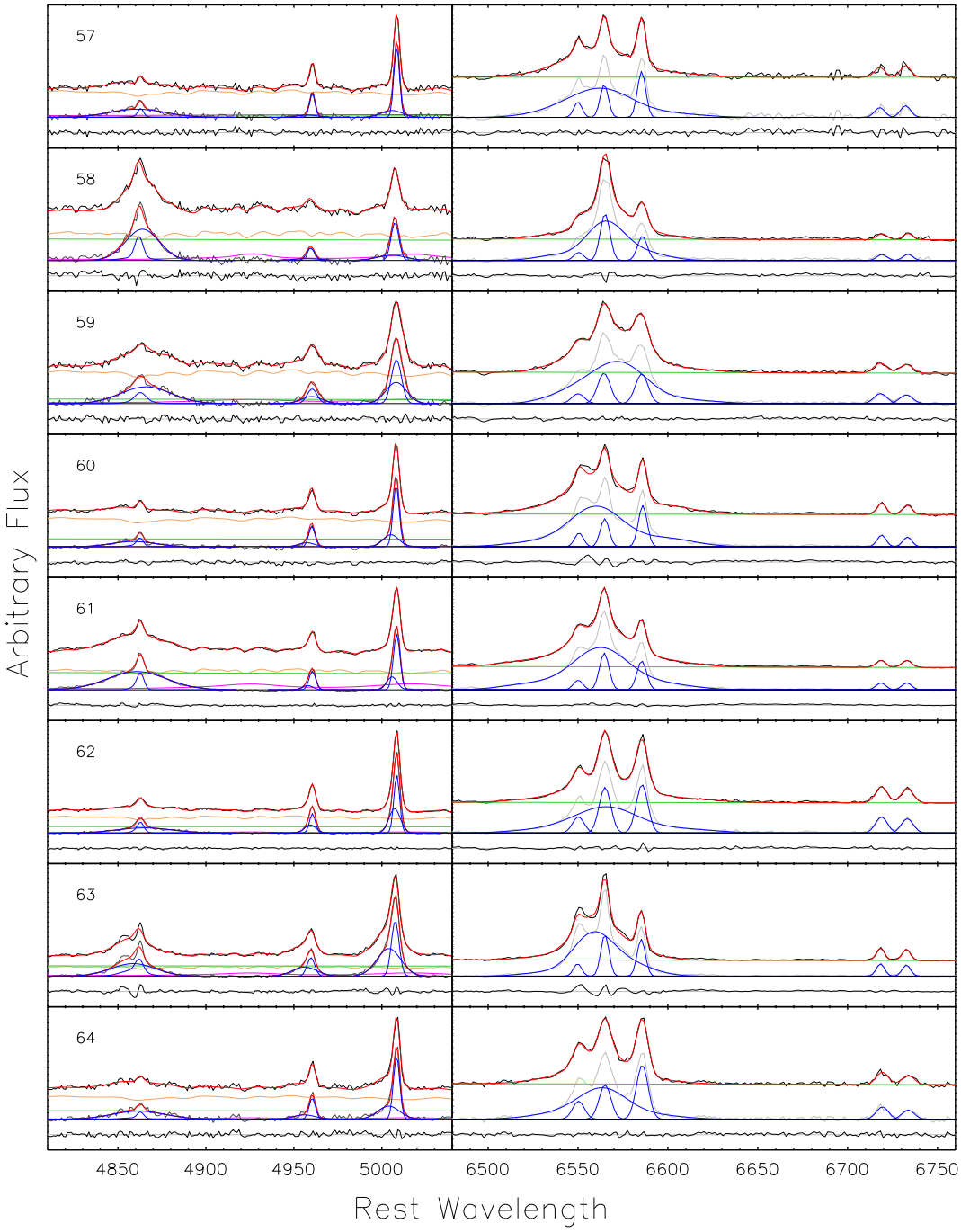

Figure 3.8: Continued

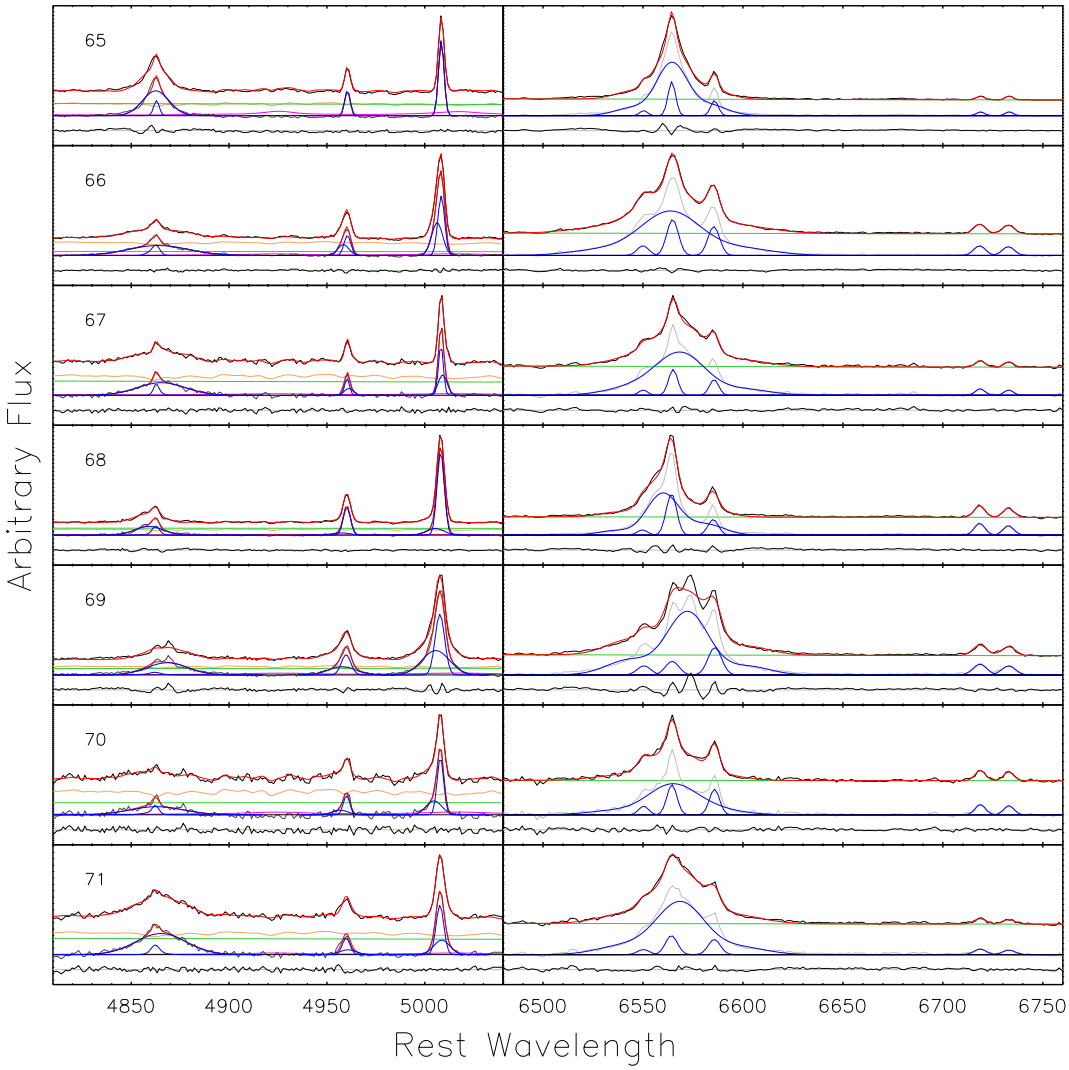

Figure 3.9: Continued

Table 3.1: The measurements of the NLS1s

No.	Objectname.	$\sigma_{\mathrm{H}\alpha}$	$\mathrm{FWHM}_{\mathrm{H}\alpha}$	$\mathrm{FWHM}_{\mathrm{H}\beta}$	$\mathrm{FWHM}_{[\mathrm{OIII}]}$	$\mathrm{FWHM}_{[\mathrm{SII}]}$	$L_{\mathrm{H}\alpha}$	$L_{5100,\mathrm{n}}$	$L_{5100,\mathrm{t}}$	R5007	$\mathrm{R4570}_{\mathrm{H}\beta}$	$\mathrm{R4570}_{\mathrm{H}\beta\mathrm{BC}}$
	(1)	(2)	(3)	(4)	(5)	(6)	(7)	(8)	(9)	(10)	(11)	(12)
1	J010409.16 + 000843.7	720	1397.63	1379	203	169	41.3	38.9	39.3	1.20	0.34	0.47
2	J030417.78 + 002827.3	742	1261.62	1536	100	182	41.3	39.0	39.3	0.55	1.19	1.30
3	J073106.86 + 392644.6	665	1185.75	1185	231	256	41.0	38.7	39.0	1.29	1.45	1.55
4	J073714.27 + 292634.2	983	1578.92	1864	216	228	41.4	39.2	39.6	1.10	1.32	1.65
5	J080253.18 + 130559.6	1074	1907.25	2454	106	188	42.0	39.6	39.7	0.55	0.14	0.15
6	J080538.22 + 244214.8	801	1349.99	1573	249	183	41.6	39.1	39.6	0.21	1.21	1.29
7	J080629.8 + 241955.6	662	1090.53	1774	181	120	40.7	38.5	39.0	0.38	0.85	1.39
8	J080801.74 + 381935.3	939	1751.07	1899	177	205	40.8	38.5	39.0	1.87	1.41	1.70
9	J081718.56 + 520147.7	866	1512.19	2107	106	151	41.0	38.6	38.9	0.77	0.57	0.69
10	J082007.8 + 372839.6	1083	1674.16	2275	207	345	41.4	39.2	39.6	0.91	2.15	3.18
11	J082912.67 + 500652.3	588	979.22	1025	155	168	41.3	38.9	39.1	1.79	0.17	0.29
12	J083202.15 + 461425.7	1041	1672.87	2344	207	184	41.4	38.8	39.5	0.40	1.27	1.37
13	J083741.94 + 263344.1	1053	1821.63	2204	123	237	41.3	39.0	39.5	0.47	0.76	0.94
14	J083949.64 + 484701.4	915	1498.42	1964	236	219	41.5	39.2	39.5	1.20	0.66	0.80
15	J084927.37 + 324852.7	1238	2082.42	3226	633	346	41.6	39.0	39.6	2.10	1.47	2.68
16	J085504.17 + 525248.3	901	1544.44	1902	369	367	41.8	39.2	39.6	0.55	0.72	0.97
17	J092438.88 + 560746.9	917	1732.27	2102	474	356	41.0	37.7	39.0	1.02	2.81	3.88
18	J093638.69 + 132529.6	997	1921.87	3075	195	406	41.4	39.1	39.6	1.46	1.33	2.33
19	J094153.41 + 163621	1027	2113.73	1905	191	208	41.0	38.4	39.0	0.78	0.04	0.06
20	J094529.36 + 093610.4	925	1787.96	2091	256	321	40.5	38.1	38.5	2.70	0.30	0.40
21	J095151.82 + 060143.7	773	1225.47	1240	211	337	40.9	39.0	39.5	1.14	1.33	1.64
22	J095848.66 + 025243.2	1035	1787.88	1955	116	120	41.0	38.8	39.5	0.71	1.54	1.79
23	J100854.93 + 373929.9	1022	1762.26	2242	189	252	42.0	39.5	39.9	0.26	0.66	0.71
24	J102532.08 + 102504	958	1649.78	2140	173	268	41.3	38.6	39.2	1.60	0.46	0.55
25	J103103.53 + 462616.8	1036	1840.75	2378	193	288	41.9	39.3	39.8	0.59	0.38	0.42
26	J103751.82 + 334850.1	1148	1990.92	2127	231	221	40.8	38.5	39.2	0.66	1.55	1.84
27	J104153.59 + 031500.6	1162	1961.49	2655	286	284	41.7	39.2	39.6	0.81	1.03	1.27
28	J105600.4 + 165626.1	1003	1839.89	2001	203	235	41.4	39.1	39.6	0.39	1.69	2.09
29	J110016.03 + 461615.2	838	1655.08	1670	161	141	40.9	38.5	39.0	2.18	0.76	1.00
30	J111031.61 + 022043.2	673	1095.00	1404	184	168	41.3	39.1	39.5	0.90	0.98	1.08
31	J111253.12 + 314807.3	1177	1794.57	2891	154	188	41.9	39.3	39.5	0.17	0.63	0.70
32	J111407.35 − 000030.9	998	1564.35	1988	208	211	41.4	39.1	39.6	0.81	1.19	1.35

Col. (1): Name of object. Col. (2): σ of Hα broad component in km s^{-1}. Col. (3): FWHM of Hα broad component in km s^{-1}. Col. (4): FWHM of Hβ broad component in km s^{-1}. Col. (5): FWHM of the core of [O III] in km s^{-1}. Col. (6): FWHM of [S II] in km s^{-1}. Col. (7): Log of Hα line luminosity in erg s^{-1}. Col. (8): Log of the AGN continuum luminosity at 5100 Å. Col. (9): Log of the monochromatic luminosity at 5100 Åwithout subtracting host galaxy and Fe II emission. Col. (10): Line flux ratio of total [O III] over total Hβ emission. Col. (11): Line flux ratio of Fe II $\lambda\lambda$4434−4684 over total Hβ emission. Col. (12): Line flux ratio of Fe II $\lambda\lambda$4434−4684 over Hβ broad component.

Table 3.2: The measurements of the NLS1s

No.	Objectname.	$\sigma_{H\alpha}$	$FWHM_{H\alpha}$	$FWHM_{H\beta}$	$FWHM_{[OIII]}$	$FWHM_{[SII]}$	$L_{H\alpha}$	$L_{5100,n}$	$L_{5100,t}$	R5007	$R4570_{H\beta}$	$R4570_{H\beta BC}$
	(1)	(2)	(3)	(4)	(5)	(6)	(7)	(8)	(9)	(10)	(11)	(12)
33	$J112229.65+214815.5$	1021	1762.41	2155	217	188	41.4	39.0	39.6	0.24	0.99	1.04
34	$J112502.62+563640.7$	1269	2062.68	2631	281	337	41.7	39.3	39.9	1.76	0.53	0.75
35	$J112526.51+022039$	907	1372.87	1671	165	205	41.0	38.7	39.2	1.52	0.98	1.19
36	$J112545.35+240823.9$	734	1269.93	1126	104	120	40.2	37.8	38.5	2.22	1.21	1.60
37	$J113101.1+134539.6$	1093	1853.28	2189	198	318	41.8	39.2	39.8	0.90	0.92	1.10
38	$J113111.94+100231.3$	985	1896.75	2677	212	381	41.2	38.8	39.5	0.47	0.24	0.28
39	$J113913.91+335551.1$	818	1377.02	1769	159	216	41.5	38.9	39.2	0.33	1.26	1.35
40	$J115333.22+095408.3$	1015	1897.43	1968	268	351	41.6	39.3	39.7	2.46	0.34	0.40
41	$J120012.47+183542.9$	990	1705.85	1363	188	230	40.9	38.8	39.3	1.60	1.44	1.69
42	$J121157.48+055801.1$	1028	2024.34	2114	218	236	41.7	39.1	39.6	0.82	0.88	0.96
43	$J122307.79+192337.1$	1108	1869.74	2264	102	166	41.3	39.1	39.6	0.52	0.62	0.68
44	$J122342.8+581446.1$	715	1042.62	1674	94	76	40.4	38.0	38.4	2.93	0.11	0.15
45	$J123651.17+453904.1$	850	1626.60	1951	116	359	41.2	38.6	39.0	1.32	0.45	0.60
46	$J123932.59+342221.3$	913	1626.01	1916	108	266	41.5	39.6	39.9	1.47	0.75	0.88
47	$J124319.98+025256.1$	770	1287.67	1668	192	204	41.7	39.5	39.8	0.92	0.44	0.55
48	$J130456.95+395529.7$	999	1643.71	1903	126	96	40.4	38.2	38.8	0.69	0.61	0.72
49	$J131142.56+331612.8$	1175	2170.30	2101	134	112	41.3	38.8	39.4	0.87	0.07	0.08
50	$J131305.8+012755.9$	921	1696.45	1908	116	80	40.8	38.2	39.1	0.73	0.69	0.76
51	$J131905.95+310852.8$	1332	2145.76	2280	176	73	40.9	38.9	39.3	1.45	0.32	0.39
52	$J134240.08+022524.3$	1009	1909.06	1941	137	237	41.0	38.8	39.4	1.06	2.02	2.69
53	$J134401.9+255628.3$	1146	1692.92	1740	175	280	41.3	38.8	39.6	1.85	1.31	1.96
54	$J140659.58+231738.7$	1080	1548.10	1400	125	93	40.7	38.8	39.3	1.03	1.45	1.68
55	$J141434.52+293428.2$	854	1391.77	1813	199	188	41.3	39.3	39.5	0.50	1.50	2.08
56	$J143658.68+164513.6$	805	1480.14	1371	81	-1	40.9	38.8	39.4	0.38	2.16	2.50
57	$J143708.46+074013.6$	1034	2089.09	2300	154	252	41.2	38.3	39.5	1.05	2.76	3.14
58	$J151356.89+481012.1$	760	1290.50	1374	273	238	41.6	39.3	39.7	0.34	1.38	1.71
59	$J152209.55+451124.1$	935	1911.76	2066	366	338	41.3	38.4	39.4	0.88	1.63	1.92
60	$J152324.42+551855.3$	1091	1749.45	1768	185	204	41.1	38.5	39.2	1.91	0.49	0.65
61	$J152940.58+302909.3$	1071	1824.20	2431	206	232	41.7	39.3	39.6	0.41	1.66	1.86
62	$J155640.9+121718$	1154	2078.84	2240	164	304	41.0	38.6	39.2	1.68	0.92	1.19
63	$J160746.01+345048.9$	752	1429.15	1811	260	180	41.5	39.2	39.4	1.37	1.37	1.96
64	$J161527.67+403153.7$	899	1652.81	2152	192	310	41.3	39.0	39.6	1.39	0.99	1.15
65	$J161809.37+361957.8$	588	908.52	962	112	120	41.1	38.9	39.2	0.56	1.61	1.81
66	$J161951.31+405847.2$	1034	1766.36	2222	180	266	41.3	38.5	39.2	1.11	0.80	0.92
67	$J162930.01+420703.2$	859	1499.45	1767	52	185	41.4	39.2	39.6	0.63	0.92	1.02
68	$J163159.59+243740.2$	653	942.96	1020	199	227	41.0	38.9	39.2	2.26	0.83	1.08
69	$J163501.45+305412.1$	868	1205.74	1509	300	324	41.6	39.1	39.5	2.30	1.31	1.41
70	$J210226.54+000702.3$	803	1485.27	1976	165	214	40.7	38.6	39.1	1.15	1.91	2.27
71	$J210533.43+002829.2$	867	1429.53	1857	222	281	41.1	38.9	39.3	0.53	0.48	0.52

Table 3.1 continued

3.2 Black hole mass

Determining $M_{\rm BH}$ using single spectra requires two quantities, line dispersion and AGN continuum luminosity. The virial mass of black hole is determined by

$$M_{\rm BH} = \frac{V_{\rm vir}^2 R}{G} = f\frac{W^2 R_{\rm BLR}}{G} \tag{3.1}$$

where V_{vir} is the virial velocity, $R_{\rm BLR}$ is the broad line region (BLR) size, W is the width of the broad line which is second moment of the line, and f is a virial coefficient (or geometrical factor) describing the BLR kinematic structure (Peterson et al. 2004). The product $W^2 R_{\rm BLR}/G$ is called the virial product. The size of $R_{\rm BLR}$ can be provided by measuring reverberation mapping (RM) lag (Onken et al. 2004; Nelson et al. 2004; Watson et al. 2008; Bentz et al. 2009a; Woo et al. 2010). From the RM observation results, a tight correlation between the measured BLR size and optical continuum luminosity was found (e.g., Kaspi et al. 2000, 2005; Bentz et al. 2009b, 2013). This size−luminosity relation provides a much less expensive way to estimate widely used to measure $M_{\rm BH}$ based on the AGN continuum luminosity (Woo & Urry 2002; Xiao et al. 2011). Consequentially, a new method using this relation, which is called single-epoch method (SE) has been widely used to measure $M_{\rm BH}$ (Greene & Ho 2005; Woo et al. 2006; Zhou et al. 2006; Komossa & Xu 2007; McGill et al. 2008; Xiao et al. 2011).

In this study, we estimated $M_{\rm BH}$ using the latest size−luminosity relation from Bentz et al. (2013),

$$\log(R_{\rm BLR}/1\ \text{lt-day}) = 1.527^{+0.031}_{-0.031} + 0.533^{+0.035}_{-0.033}\ \log(\lambda L_\lambda/10^{44}\ \text{erg s}^{-1}) \tag{3.2}$$

where L_λ is continuum luminosity at ∼5100Å. Using the Hα line than the Hβ line is more suitable due to low quality spectra of Hβ region, hence we converted the line

width and the line luminosity of Hα to the Hβ line width and the continuum luminosity with following two relations from Greene & Ho (2005). First, the $\sigma_{\rm H\alpha}$ is converted to the $\sigma_{\rm H\beta}$ using the equation 3.3 on an assumption of same ratio of FWHM/$\sigma_{\rm line}$ for both Hα and Hβ.

$$\mathrm{FWHM_{H\beta}} = (1.07 \pm 0.07) \times 10^3 \left(\frac{\mathrm{FWHM_{H\alpha}}}{10^3 \text{ km s}^{-1}} \right)^{(1.03\pm0.03)} \text{ km s}^{-1} \tag{3.3}$$

Second, the continuum luminosity, L_{5100}, is obtained from Hα line luminosity by using the empirical relation.

$$L_{\rm H\alpha} = (5.25 \pm 0.02) \times 10^{42} \left(\frac{\lambda L_{5100}}{10^{44} \text{ erg s}^{-1}} \right)^{(1.157\pm0.005)} \text{ erg s}^{-1} \tag{3.4}$$

We derived a black hole mass estimator by combining with the virial relation (Eq. 3.1). By adopting the virial coefficient f=5.1 from Woo et al. (2013), the derived estimator is given as:

$$M_{\rm Y\alpha} = f \times 10^{6.544} \left(\frac{L_{\rm H\alpha}}{10^{42} \text{ erg s}^{-1}} \right)^{0.46} \left(\frac{\sigma_{H\alpha}}{10^3 \text{ km s}^{-1}} \right)^{2.06} \text{ M}_\odot \text{ ,} \tag{3.5}$$

and we will denote the derived estimator as $M_{\rm Y\alpha}$.

Accurate measurements of black hole mass as well as σ_* are important to investigate the $M_{\rm BH}-\sigma_*$ relation of NLS1s. To investigate the uncertainties of $M_{\rm BH}$, we determined $M_{\rm BH}$ with three more ways and compare them with the $M_{\rm Y\alpha}$. First, the latest black hole mass estimator based on $\sigma_{\rm H\alpha}$ and $L_{\rm H\alpha}$ from McGill et al. (2008) expressed is used.

$$M_{\rm M\alpha} = f \times 10^{6.465} \left(\frac{L_{\rm H\alpha}}{10^{42} \text{ erg s}^{-1}} \right)^{0.55} \left(\frac{\sigma_{H\alpha}}{10^3 \text{ km s}^{-1}} \right)^{2} \text{ M}_\odot \tag{3.6}$$

Secondly, we measured $M_{\rm BH}$ with following equation from Greene & Ho (2005) to compare with $M_{\rm BH}$ based on $\mathrm{FWHM_{H\alpha}}$ measurement and the mass is expressed by

$M_{\mathrm{GH}\alpha}$.

$$M_{\mathrm{GH}\alpha} = f \times 10^{5.82} \left(\frac{L_{\mathrm{H}\alpha}}{10^{42}\ \mathrm{erg\ s^{-1}}}\right)^{0.55} \left(\frac{\mathrm{FWHM}_{\mathrm{H}\alpha}}{10^{3}\ \mathrm{km\ s^{-1}}}\right)^{2.06} \mathrm{M}_{\odot} \tag{3.7}$$

Lastly, we obtained the M_{BH} by using Hβ for some of the NLS1s showing higher S/N of Hβ than 20. The following equation from Park et al. (2012) is used for the black hole mass with Hβ measurements denoted by $M_{\mathrm{P}\beta}$.

$$M_{\mathrm{P}\beta} = f \times 10^{6.623} \left(\frac{\lambda L_{5100,n}}{10^{44}\ \mathrm{erg\ s^{-1}}}\right)^{0.518} \left(\frac{\sigma_{\mathrm{H}\beta}}{1000\ \mathrm{km\ s^{-1}}}\right)^{2.212} \mathrm{M}_{\odot} \tag{3.8}$$

where $L_{5100,n}$ is the AGN continuum luminosity at 5100Å measured with ±20Å window after subtracting host-galaxy starlight and Fe II emission from the raw spectrum.

The comparisons between the M_{BH} measurements in this study is illustrated in Figure 3.10. $M_{\mathrm{Y}\alpha}$ is systemically greater than $M_{\mathrm{M}\alpha}$ by -0.145 dex with ± 0.004 dex error. The same width and flux of Hα are used to both $M_{\mathrm{Y}\alpha}$ and $M_{\mathrm{M}\alpha}$, the difference only shows the different exponents of two equations. The equation 3.6 for $M_{\mathrm{M}\alpha}$ was established in somewhat higher mass range around $10^8 - 10^9\ M_{\odot}$, therefore a small variation of the exponent could result in quite big difference when it is used for lower mass range around $10^6 - 10^7\ M_{\odot}$ as the mass range of the NLS1s. Moreover, in the study of McGill et al. (2008), Hα modeled without removal of the [N II] and Hα narrow component, and the total flux of Hα was used while we used only the flux of Hα broad component after subtracting both [N II] doublet and Hα narrow component. The NLS1s tend to show weaker and narrower Balmer lines than BL AGNs as in McGill et al. (2008), thus not only the Hα narrow component but also the [N II] doublet could affect the Hα measurements more than BL AGNs. In consideration of these uncertainties, the offset could be embraceable.

Meanwhile, $M_{\mathrm{GH}\alpha}$ and $M_{\mathrm{P}\beta}$ have fairly lower mass than $M_{\mathrm{Y}\alpha}$ by -0.309 ± 0.021 dex and -0.461 ± 0.021 dex, respectively. The difference between $M_{\mathrm{Y}\alpha}$ and $M_{\mathrm{GH}\alpha}$ can be explained as follows. NLS1s in this study have low ratio of $\sigma_{\mathrm{H}\alpha}$ to $\mathrm{FWHM}_{\mathrm{H}\alpha}$ ranging

1.39−2.06 with an average of 1.73, i.e., our sample tends to have somewhat larger $\sigma_{\mathrm{H}\alpha}$ relative to $\mathrm{FWHM}_{\mathrm{H}\alpha}$. Therefore, $M_{\mathrm{GH}\alpha}$ with $\mathrm{FWHM}_{\mathrm{H}\alpha}$ could be underestimated relative to $M_{\mathrm{Y}\alpha}$ with $\sigma_{\mathrm{H}\alpha}$. By the way, H$\alpha$ emission lines have tendency to show asymmetric profiles and wings, thus $\sigma_{\mathrm{H}\alpha}$ measurements is more trustworthy than $\mathrm{FWHM}_{\mathrm{H}\alpha}$, and that is $M_{\mathrm{Y}\alpha}$ is more reliable than $M_{\mathrm{GH}\alpha}$. In addition, as with the case of the equation of $M_{\mathrm{M}\alpha}$, the different mass range between when the equation is developted and when the equation is applied can be one more reason here again. For the case of the difference of $M_{\mathrm{P}\beta}$ from $M_{\mathrm{Y}\alpha}$, however, much more important reason could be the differences between the Hα and Hβ measurements. In this context, the bad quality of Hβ region (average S/N ∼25) and the weakness of Hβ would be the main factors to cause the differences of measurements. Besides, Hα broad component was modeled with Gauss-Hermite series whereas Hβ was modeled with single Gaussian because of low quality of Hβ spectra. Single Gaussian profile is not suitable to fit wing and asymmetry of emission, so $\sigma_{\mathrm{H}\beta}$ could be underestimated. This result could make $M_{\mathrm{P}\beta}$ have lower mass than $M_{\mathrm{Y}\alpha}$. In other words, the different fitting method for Hα and Hβ cased the mass difference between $M_{\mathrm{Y}\alpha}$ and $M_{\mathrm{P}\beta}$. As discussed above, the measurement of M_{BH} has fairly big uncertainties according to different methods. The major reason would be the peculiarity of broad Balmer lines, e.g., the weakness or absence of of Hβ emission which is not enough to measure M_{BH} and this one of limitations of this study.

Eddington ratios, represented by $L_{\mathrm{bol}}/L_{\mathrm{Edd}}$, were calculated from the $M_{\mathrm{Y}\alpha}$, according to equation 3.9. For the bolometric luminosity, L_{bol}, we assumed $L_{\mathrm{bol}} = 9\lambda L_{5100}$ (Kaspi et al. 2000; Peterson et al. 2004).

$$L/L_{\mathrm{Edd}} = \frac{L_{bol}}{1.25 \times 10^{38} \times M_{\mathrm{BH}}} \tag{3.9}$$

As a result, we found that our NLS1 galaxies have the M_{BH} with the range $\log M_{\mathrm{BH}}$= 6.13−7.33 and an average value of 6.84. It confirms the well-known result that NLS1s have lower M_{BH} than BL AGNs as reported by Grupe (2004); Komossa & Xu (2007).

Komossa & Xu (2007) found the black hole mass of NLS1s range log$M_{\rm BH}$= 5.3−7.3 $M_{\odot}$, while the black hole mass of BLS1s range log$M_{\rm BH}$= 6.5−8.4 $M_{\odot}$. These show our NLS1s have lower black hole mass than BL AGNs. The Eddington ratio of our NLS1s ranges from 0.04 to 0.35 with an average of 0.14. This result does not similar previous results of Komossa & Xu (2007) with $L/L_{\rm Edd}$ = 0.25−1.99 (the average is 0.79) for NLS1s and with $L/L_{\rm Edd}$ = 0.04−0.50 (the average is 0.16) for BLS1s. Komossa & Xu (2007) calculated the $M_{\rm BH}$ with Hβ and L_{5100} measurements while we used Hα measurements, thus there could be a systematic difference in the $M_{\rm BH}$ measurements and this could result in the difference in the $L/L_{\rm Edd}$.

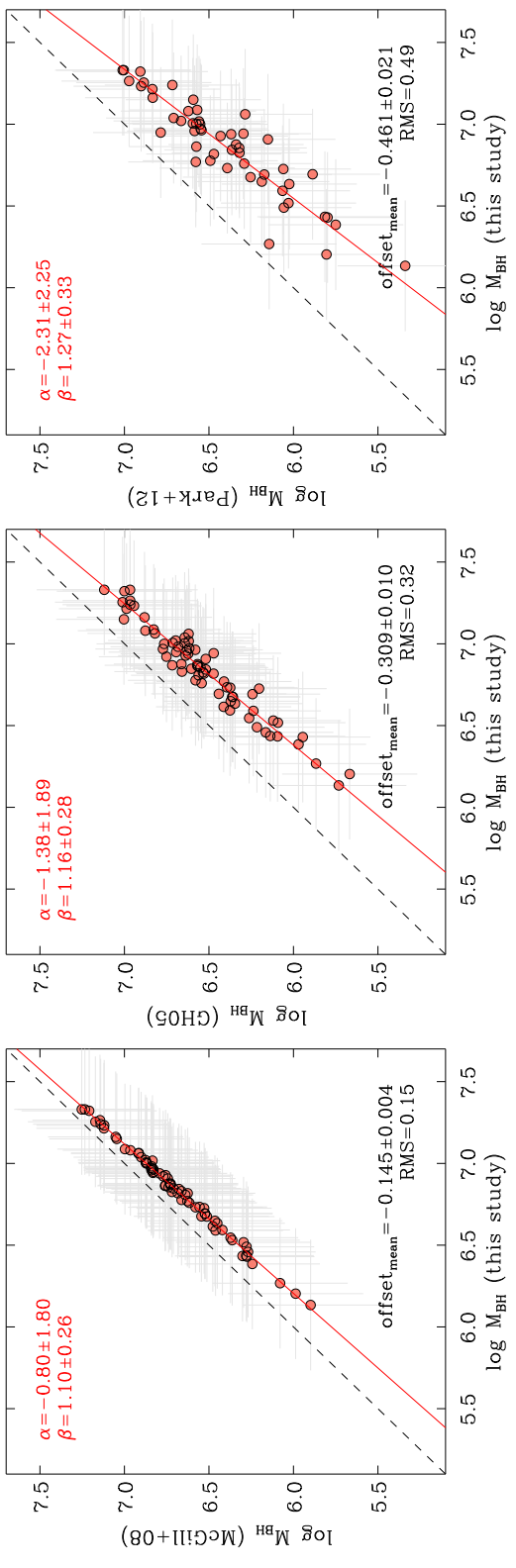

Figure 3.10: Black hole mass comparisons of $M_{\mathrm{Y}\alpha}$ with $M_{\mathrm{M}\alpha}$, $M_{\mathrm{GH}\alpha}$, and $M_{\mathrm{P}\beta}$ from left to right. For $M_{\mathrm{P}\beta}$, only high quality targets (S/N of H$\beta > 20$) are expressed. The red solid line shows the best-fit of the comparison.

3.3 Stellar velocity dispersion

Measuring stellar velocity dispersions precisely is one of the most important processes to determine the location of NLS1 on the $M_{\rm BH}-\sigma_*$ plane. To obtain reliable measurements of σ_*, we measured σ_* by three ways in two regions: (1) in Mg b region by using Mg b triplet (5069, 5154, 5160Å) and Fe (5270, 5335Å) absorption lines (hereafter $\sigma_{\rm Mgb}$); (2) in the same region by using only Fe lines without Mg b triplet (hereafter $\sigma_{\rm noMgb}$); and (3) in Ca II region by using Ca II triplet (8498, 8542, 8662Å) absorption lines (hereafter $\sigma_{\rm CaT}$). The Mg b triplet, which is an $\alpha-$element, is much deeper in the composite spectra of massive elliptical galaxies than in the stellar template hence the template mismatch due to the different of $\alpha-$element can cause a systematic bias in measuring σ_* (Barth et al. 2002, 2003; Woo et al. 2004, 2005, 2006). To consider the effect of Mg b triplet, we compared $\sigma_{\rm Mgb}$ with $\sigma_{\rm noMgb}$. The Ca II triplet region is expected to be less sensitive to stellar population variations and AGN contamination from emission lines than the Mg b region, and thus provides more reliable measurements of the velocity dispersion. Thus the $\sigma_{\rm CaT}$ was used to test the consistency of the $\sigma_{\rm Mgb}$.

After masking out AGN narrow emission lines (e.g., [Fe VII] λ5160, [N I] λ5201, [Ca V] λ5310 etc.; Vanden Berk et al. 2001), we measured σ_* by using Python-based code *vdfit* from (van der Marel 1994) that employs Bayesian statistical estimation using Markov Chain Monte Carlo sample with a set of stellar templates. The set of stellar templates was taken from INDO$-$US stellar library containing spectra of four K giants, three G giants, an F2 and an A0 giants (Valdes et al. 2004). We used 1$-$4 orders of polynomials to model the continuum. After considerable tests were carefully conducted for each target with a number of combinations of various polynomial orders and fitting ranges, σ_* was determined by taking the mean value of the various measurements. The fitting results are shown in Figure 3.11$-$19.

In summary, we obtained $\sigma_{\rm Mgb}$ for 71 NLS1s showing strong enough stellar lines. Among them, we were able to measure σ_* for 34 NLS1s in the Ca II region since the Ca II

triplet was not included in the SDSS spectral range for higher z AGNs or the Ca II triplet is too weak to measure σ_*. The results of comparing the three different measurements of σ_* are presented in Figure 3.20. The $\sigma_{\rm Mgb}$ is slightly higher by -0.015 ± 0.007 dex than the $\sigma_{\rm noMgb}$ and the rms scatter is small as 0.06 dex. This result confirms the $\sigma_{\rm Mgb}$ is consistent with the $\sigma_{\rm noMgb}$ and indicates the influence of the Mg b triplet in measuring the σ_* is marginal for the host galaxies of NLS1s. Compared to the $\sigma_{\rm CaT}$, the $\sigma_{\rm Mgb}$ shows slightly larger scatter (0.10 dex) than the $\sigma_{\rm noMgb}$, but the average offset is still close to zero by -0.014 ± 0.016 dex. As seen in this result, the $\sigma_{\rm Mgb}$ is consistent with the $\sigma_{\rm CaT}$. Additionally, the relation between the $\sigma_{\rm noMgb}$ and $\sigma_{\rm CaT}$ has 0.008 ± 0.015 dex offset with 0.09 rms scatter, thus this shows that the $\sigma_{\rm noMgb}$ and $\sigma_{\rm CaT}$ are also consistent. Based on these comparisons, which did not show strong bias among them, we adopted $\sigma_{\rm Mgb}$ as the final measurements.

Six of our NLS1s were studied previously by Xiao et al. (2011) hence σ_* measurements based on high quality spectra are available. Spectra in their study were obtained with the Keck Echellette Spectropragh and Imager (ESI) and the Magellan Echellette (MagE), thus the quality of data is better than the SDSS spectra and the results are more reliable. For this reason, we adopted the results of Xiao et al. (2011) for the six targets. We finally used 71 measurements of the $\sigma_{\rm Mgb}$ including the σ_* measurements of Xiao et al. (2011). In general, the σ_* of Xiao et al. (2011) and this study are consistent within error range, but minor difference could be caused by differences of the aperture size. The SDSS fiber size is 3" which is larger than slit size of the Keck and Magellan telescopes. Hence the SDSS spectra include larger area in the disk than Xiao et al. (2011). Consequently, the influence of galaxy disk component may result in the difference of σ_*. The measurements of these six sample is listed in Table 3.3.

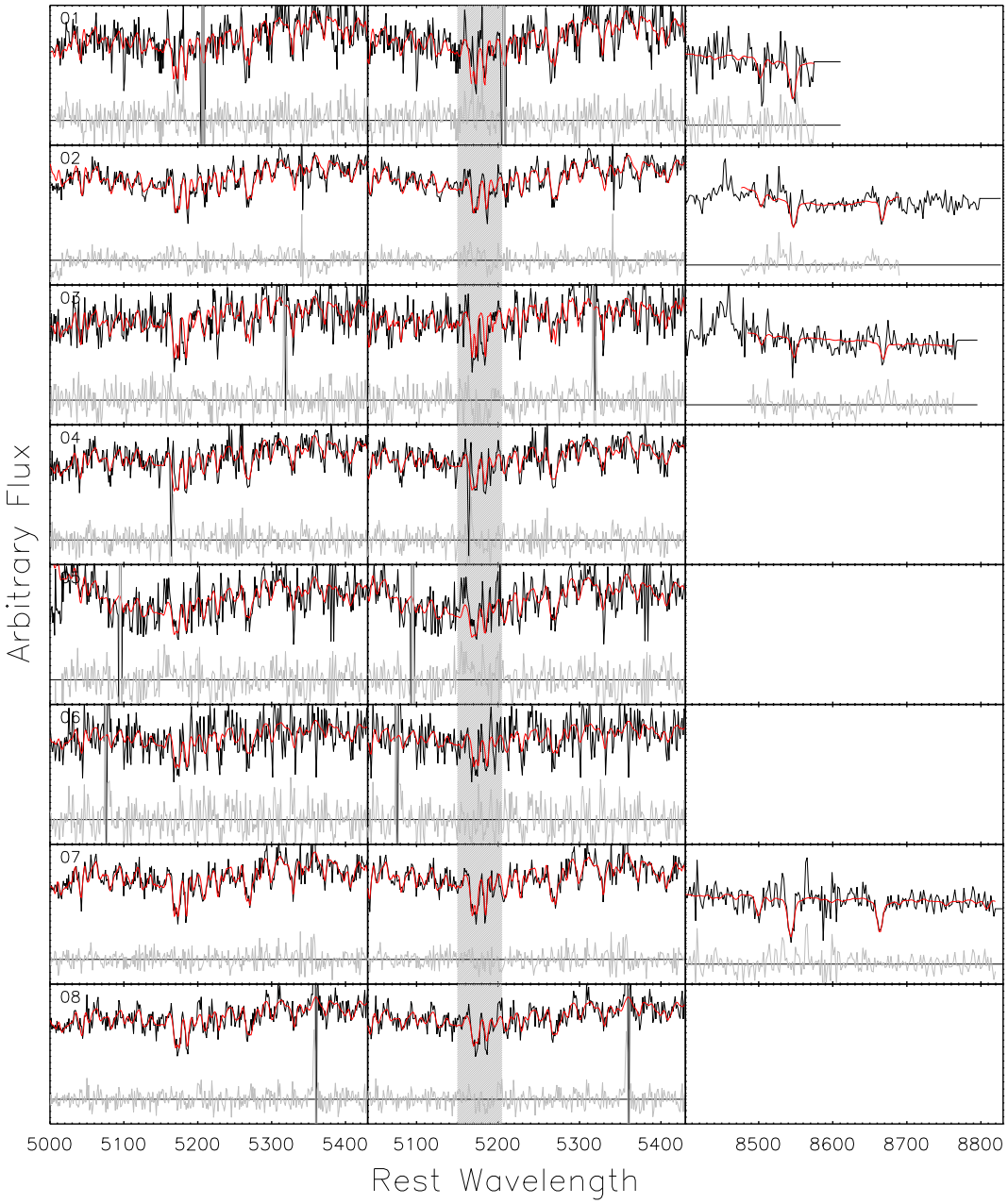

Figure 3.11: Stellar velocity dispersion measurements by three ways in two regions; (1) Mg *b* region with Mg *b* triplet (left), (2) Mg *b* region without Mg *b* triplet (middle), and (3) Ca II region with Ca II triplet (right). In each panel, stellar spectrum (black) and best-fit model (red) are shown in the upper part, and the residuals (light gray) showing the difference between the spectrum and the best-fit model is presented in the lower part. The region masked out is expressed by gray shaded bands.

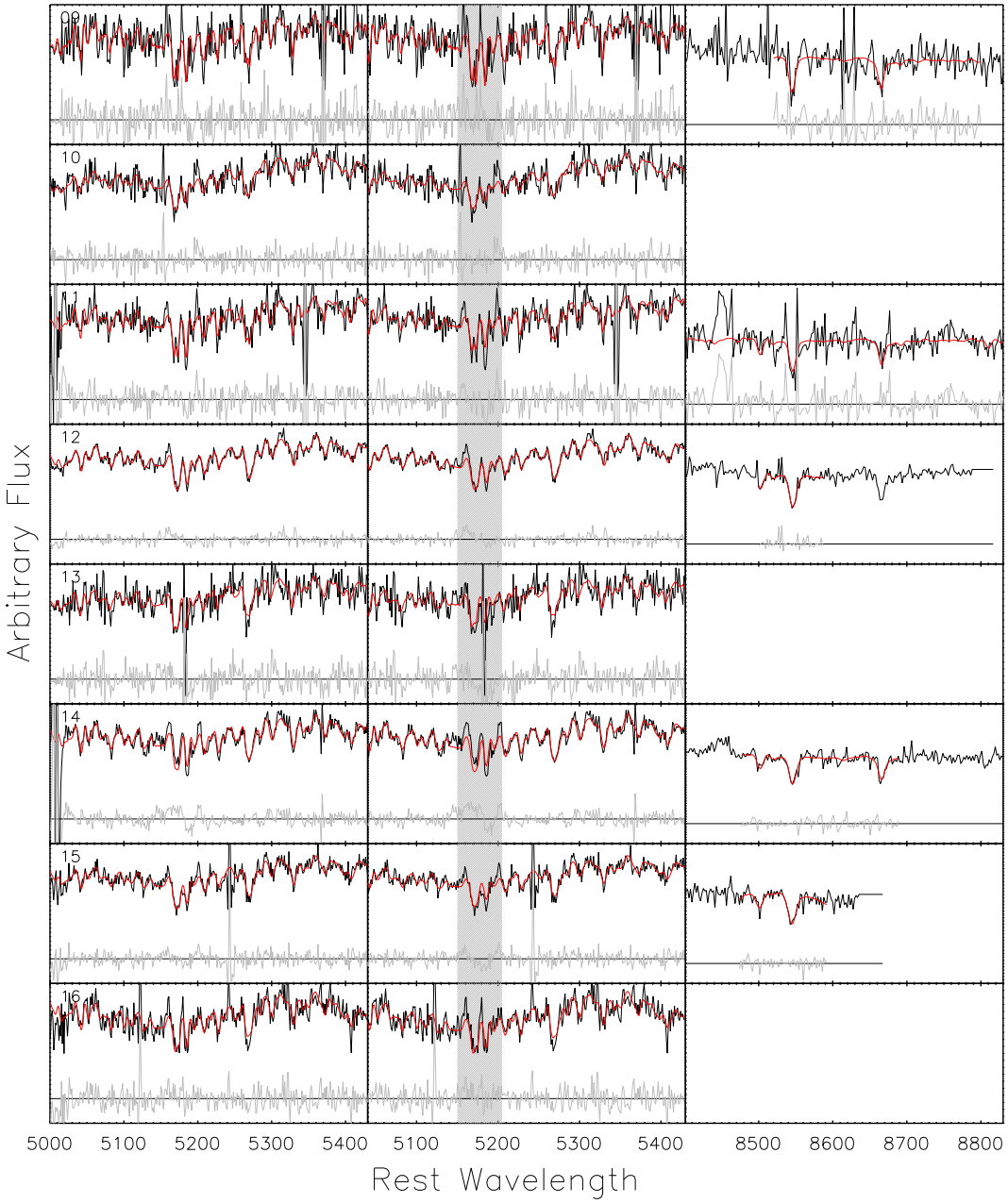

Figure 3.12: Continued

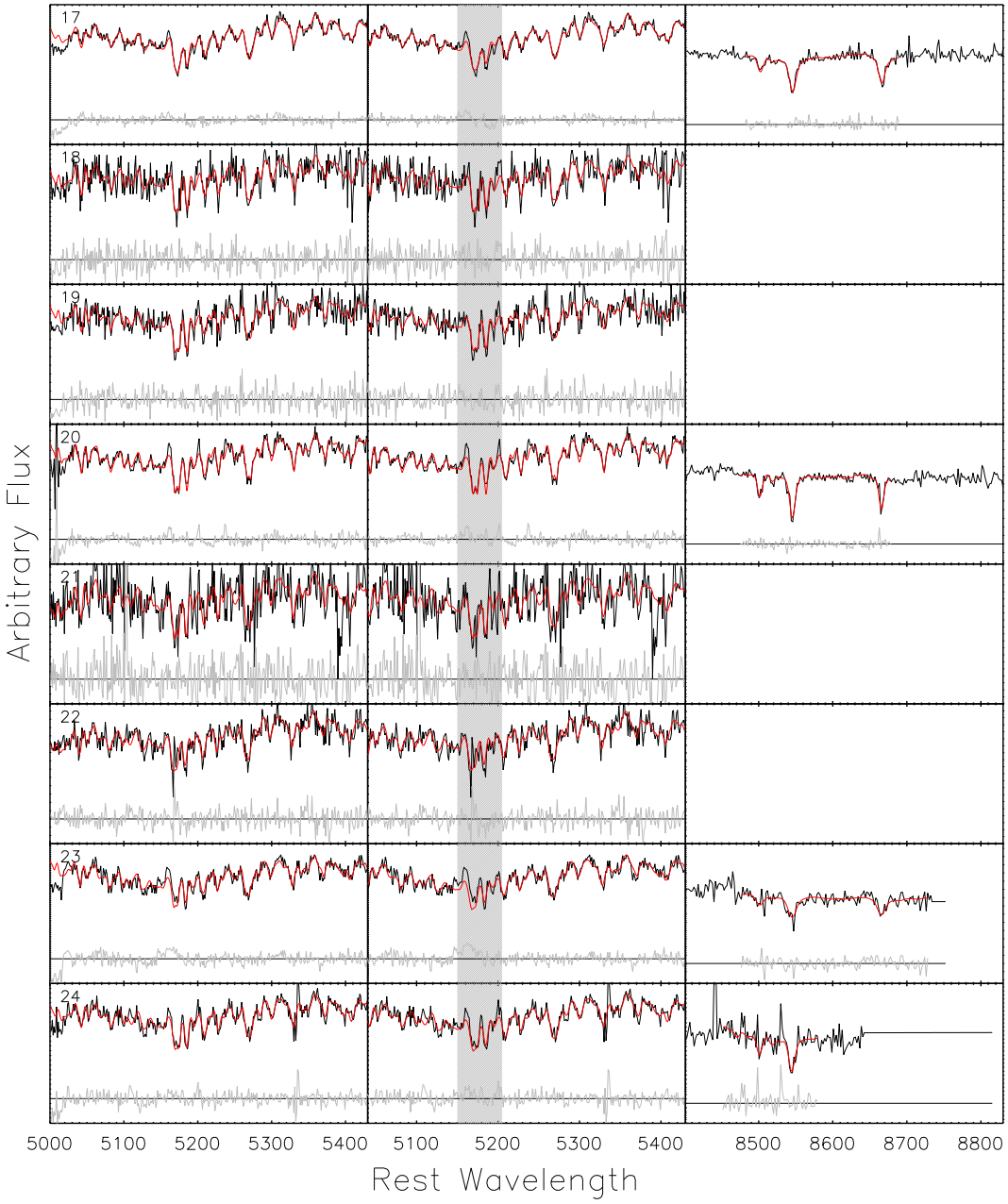

Figure 3.13: Continued

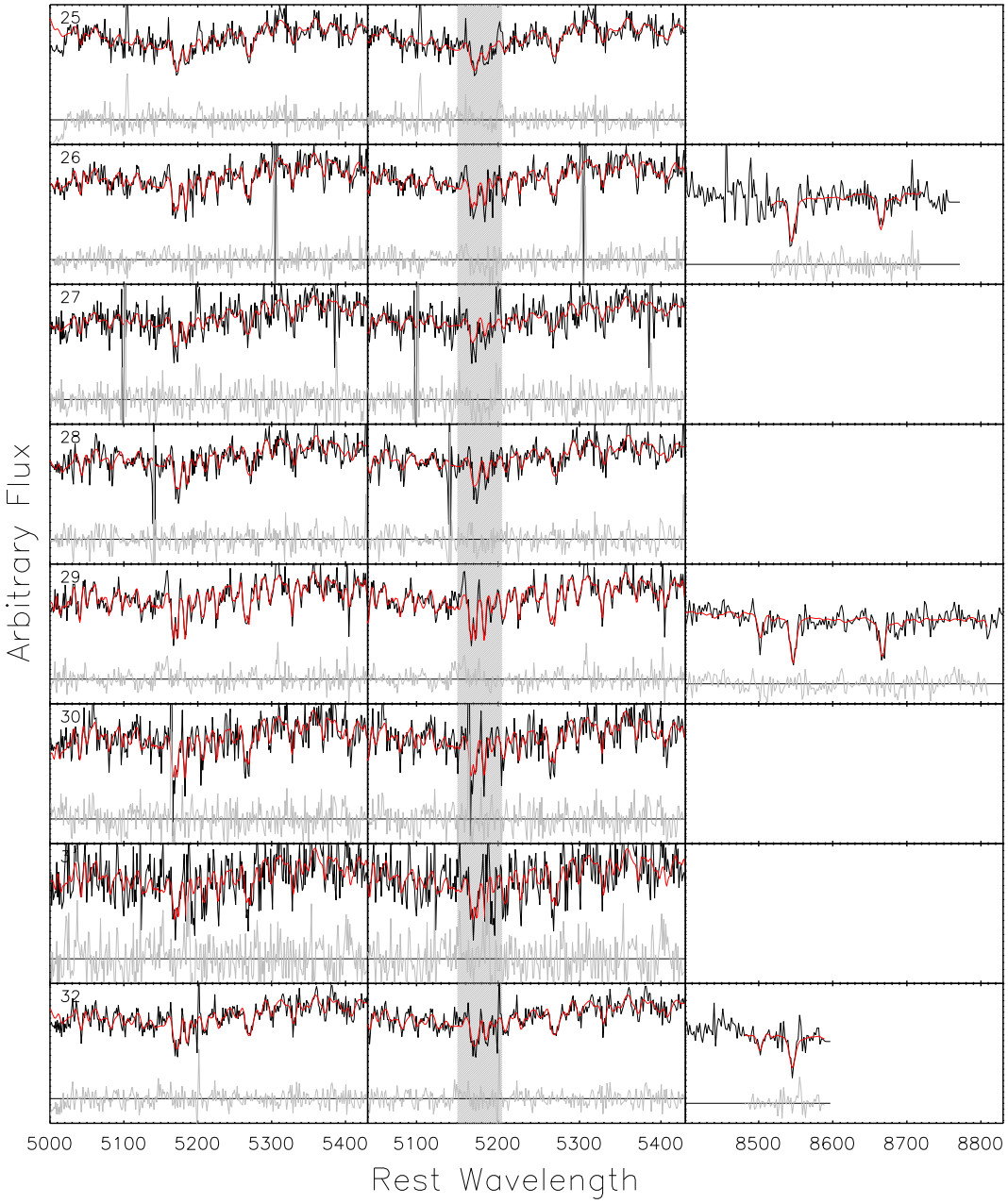

Figure 3.14: Continued

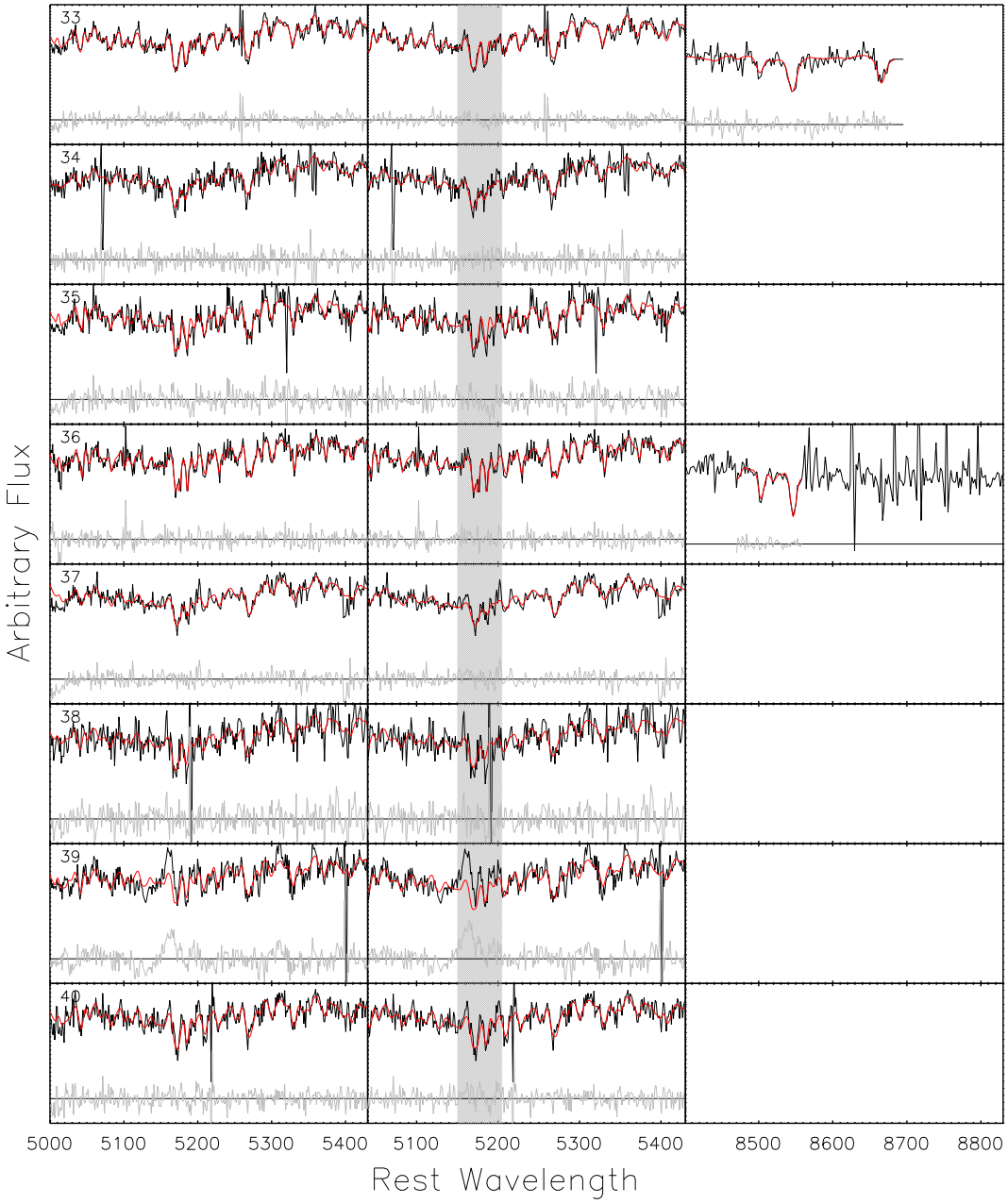

Figure 3.15: Continued

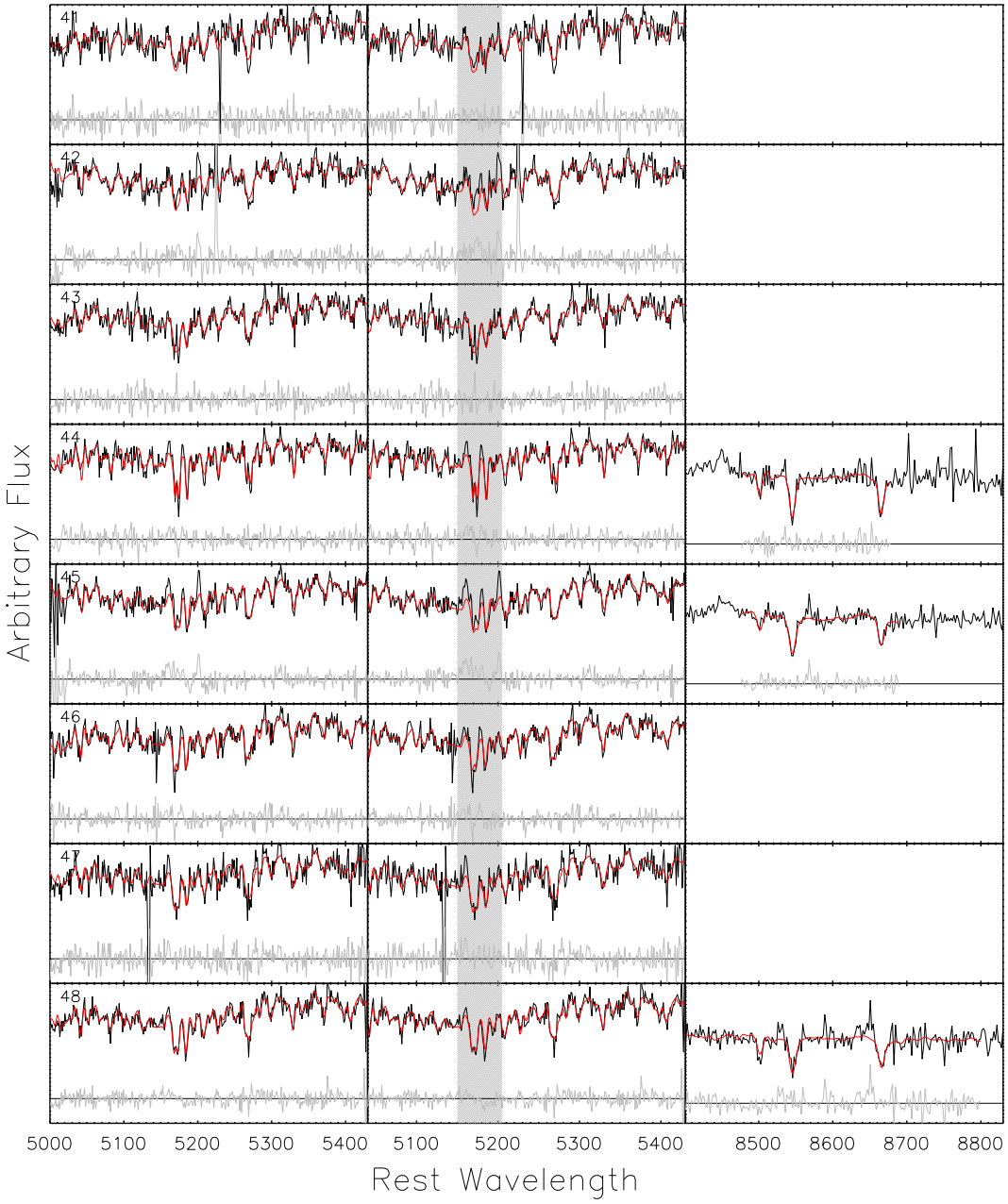

Figure 3.16: Continued

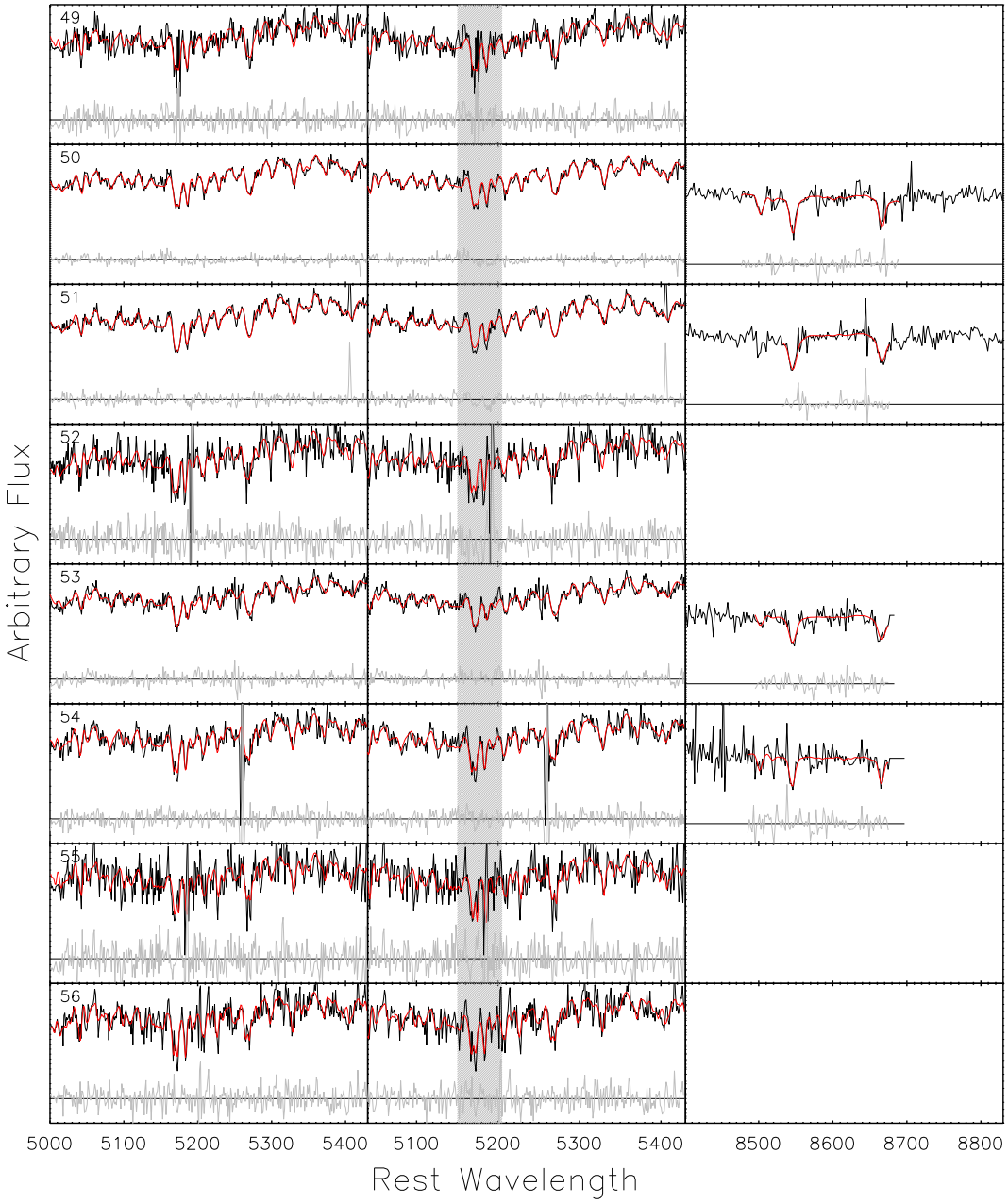

Figure 3.17: Continued

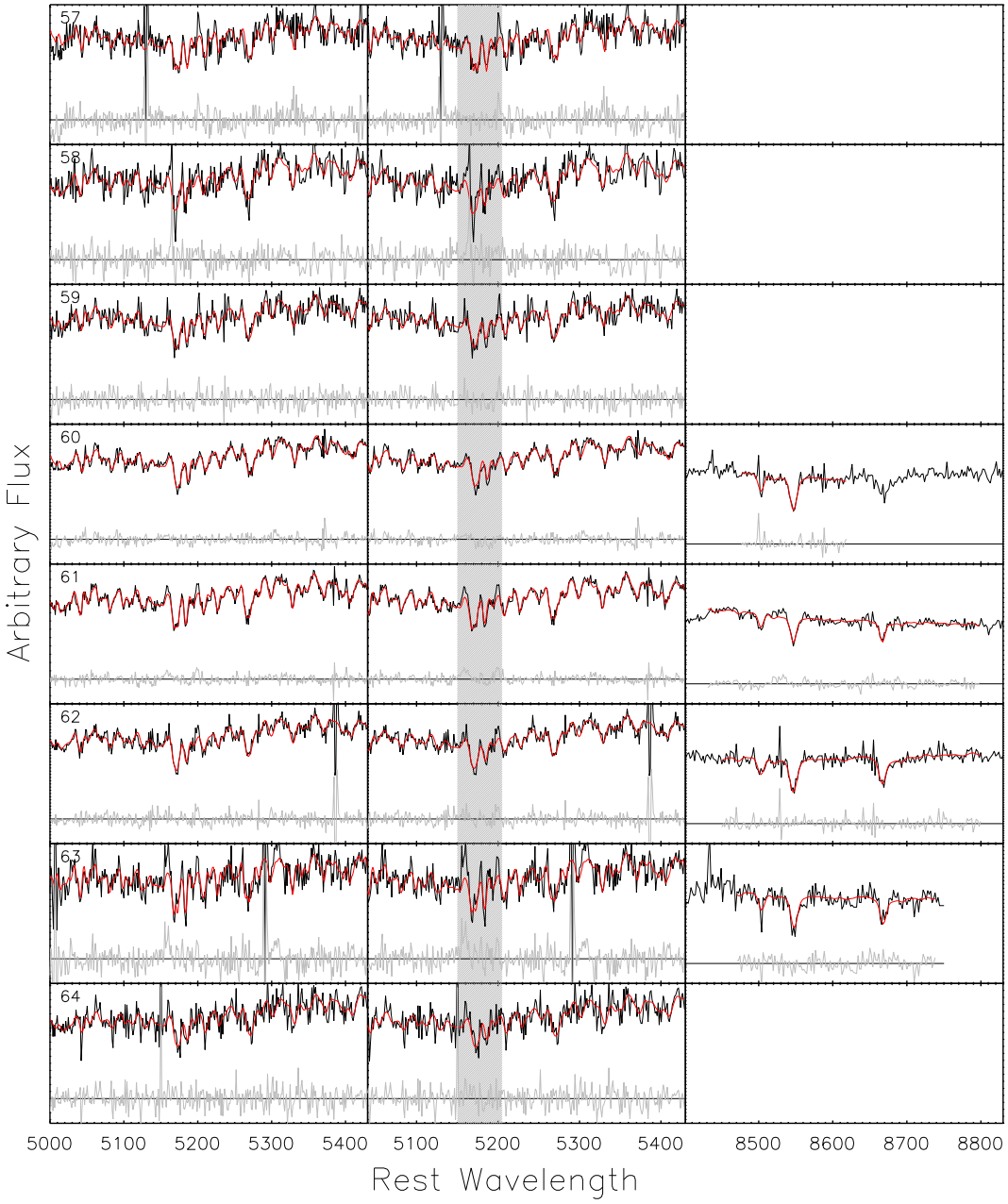

Figure 3.18: Continued

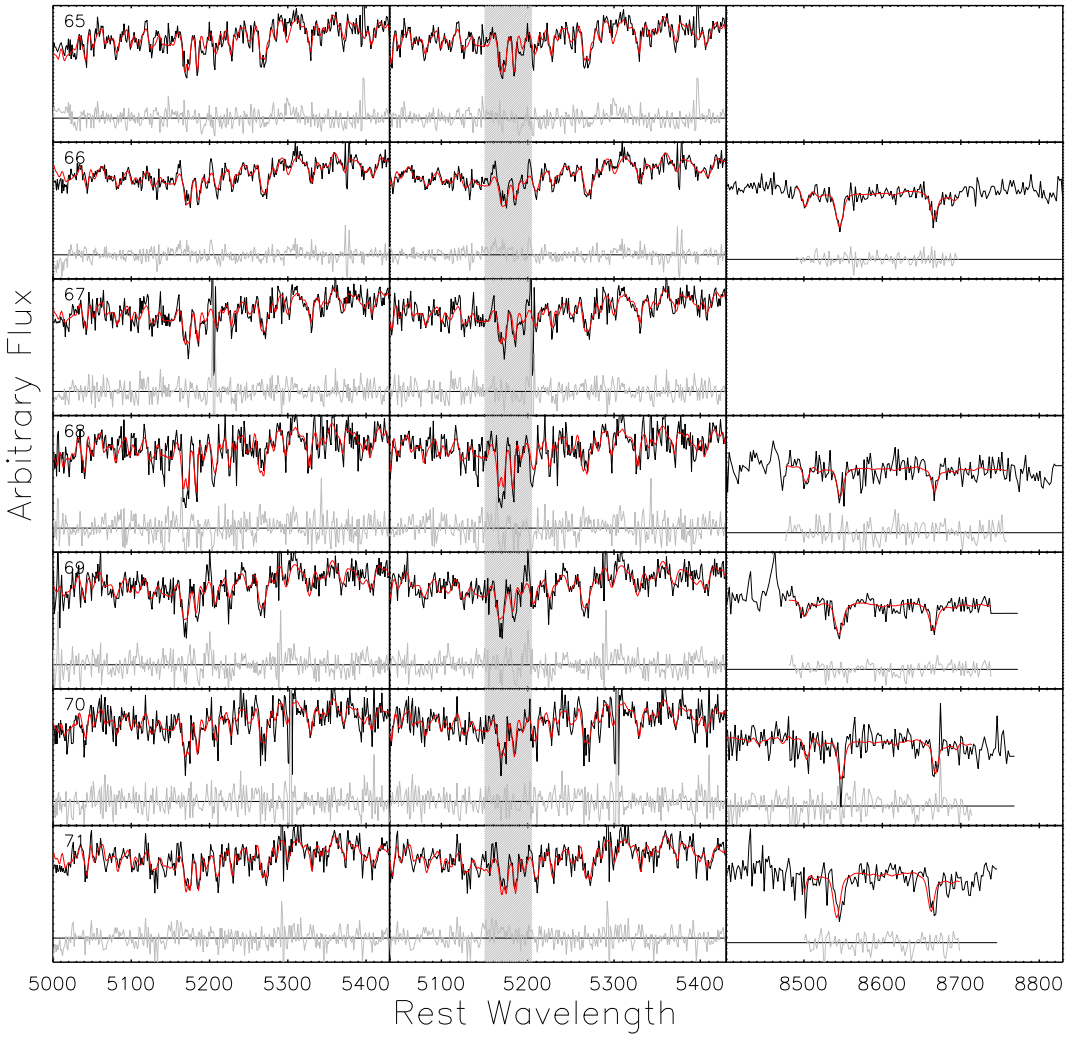

Figure 3.19: Continued

Table 3.3: List of the sample from Xiao et al. (2011)

Objectname (1)	σ_* (Xiao+11)(2)	σ_* (this study)(3)	z (4)	Size (Xiao+11)(5)	Slit width (6)	Size (SDSS)(7)
$J080629.8+241955.6$	71 ± 5	72 ± 12	0.042	0.61	0.75”	2.45
$J082912.67+500652.3$	60 ± 2	66 ± 11	0.043	0.63	0.75”	2.51
$J094529.36+093610.4$	76 ± 2	67 ± 8	0.013	0.26	1”	0.79
$J095151.82+060143.7$	76 ± 6	81 ± 18	0.093	1.71	1”	5.12
$J111031.61+022043.2$	77 ± 3	68 ± 12	0.080	1.49	1”	4.47
$J122342.8+581446.1$	45 ± 2	54 ± 3	0.015	0.23	0.75”	0.91

Col. (1): Name of object. Col. (2): Stellar velocity dispersion from Xiao et al. (2011) in km s^{-1}. Col. (3): Stellar velocity dispersion in this study in km s^{-1}. Col. (4): Redshift. Col. (5): Physical size corresponding to the study of Xiao et al. (2011) in kpc. Col. (6): Slit size for the observation of Xiao et al. (2011). Col. (7): Physical size corresponding to the SDSS fiber size (3”) in kpc.

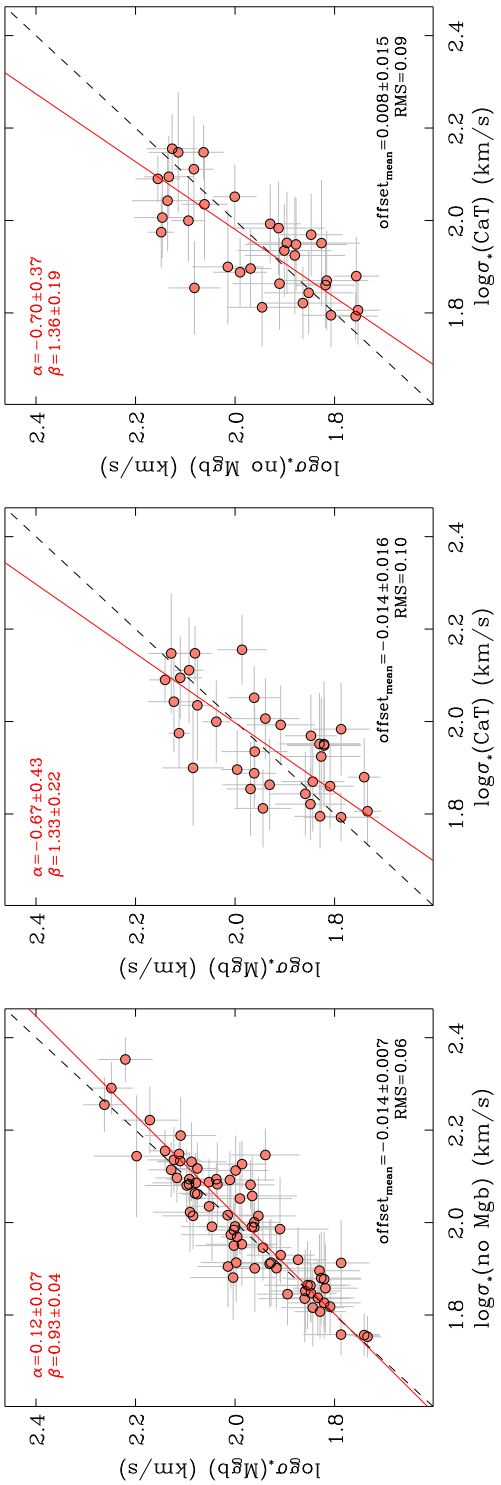

Figure 3.20: Comparisons between the measurements of stellar velocity dispersions of Mg b, no Mg b, and CaT. The number of measurements is 71 for both $\sigma_{\rm Mgb}$ and $\sigma_{\rm noMgb}$, and 34 for $\sigma_{\rm CaT}$. The best line-fit (red solid line) is representing trend between two measurements.

3.4 Morphology classification

In case of galaxies with rotating galactic disk, the line-of-sight stellar velocity dispersion can be overestimated due to rotational broadening (Bennert et al. 2011; Harris et al. 2012; Kang et al. 2013), therefore it is important to correct the rotation effect in measuring σ_*. The rotating disks are more frequently shown in late type galaxies than in early type galaxies, i.e., the rotation effect is stronger for late type galaxies than for early type galaxies. Among the late type galaxies, more incline galaxies to the line-of-sight will suffer more bias in the velocity dispersion.

To investigate the rotation effect on the σ_*, we classified our NLS1s into early types and late types by colors and existence of the galactic disk, and we further divided the late galaxies into face-on late types and edge-on late types according to galactic inclination. Assuming the disk is fundamentally circular symmetry, we determined the inclination angle of the galactic disk by using the axial ratio of the disk with following equation, $i = sin^{-1}q$ where i is the inclination angle of the galactic disk to the line of sight (defined so that $i = 90^\circ$ for a face-on disk) and q is the axial ratio which is the ratio between major and minor axes in the SDSS image. We classified our sample with $q > 0.5$ as face-on galaxies, and the others with $q < 0.5$ were classified as edge-on galaxies. As a result, 71 NLS1 galaxies were divided into 28 early type galaxies and 43 late type galaxies which were further divided into 34 face-on and 9 edge-on late types. The classification of the NLS1s is listed in the column (11) and (12) of Table 2.1.

Chapter 4

Result

4.1 The $M_{\rm BH} - \sigma_*$ relation

Conventionally, the $M_{\rm BH} - \sigma_*$ relation is expressed as

$$\log\left(M_{\rm BH}/M_{\odot}\right) \;=\; \alpha \;+\; \beta \;\log\left(\sigma_*/200{\rm km\ s^{-1}}\right). \tag{4.1}$$

To compare the NLS1s with the other types of AGNs and normal galaxies, we use the results on the $M_{\rm BH} - \sigma_*$ relations of 25 reverberation−mapped AGNs (Woo et al. 2013) and of 72 normal galaxies McConnell & Ma (2013). For a reverberation mapping sample of active galaxies, the best-fit was determined as $\alpha = 7.31 \pm 0.15$ and $\beta = 3.46 \pm 0.61$. Meanwhile, McConnell & Ma (2013) divided 72 normal galaxies into late type and early type galaxies, finding $\alpha = 8.07 \pm 0.21$, $\beta = 5.06 \pm 1.16$ for late type galaxies and $\alpha = 8.39 \pm 0.06$, $\beta = 5.20 \pm 0.36$ for early type galaxies.

We present the result of the $M_{\rm BH} - \sigma_*$ relation of the NLS1s in Figure 4.1 by dividing our sample into three groups according to morphology classification as explained in section 3.4. The NLS1s are compared to the $M_{\rm BH} - \sigma_*$ relation of the RM AGNs and the normal galaxies on $M_{\rm BH} - \sigma_*$ plane, and the result for the offset from the slopes compared to $L/L_{\rm Edd}$ are shown in Figure 4.2.

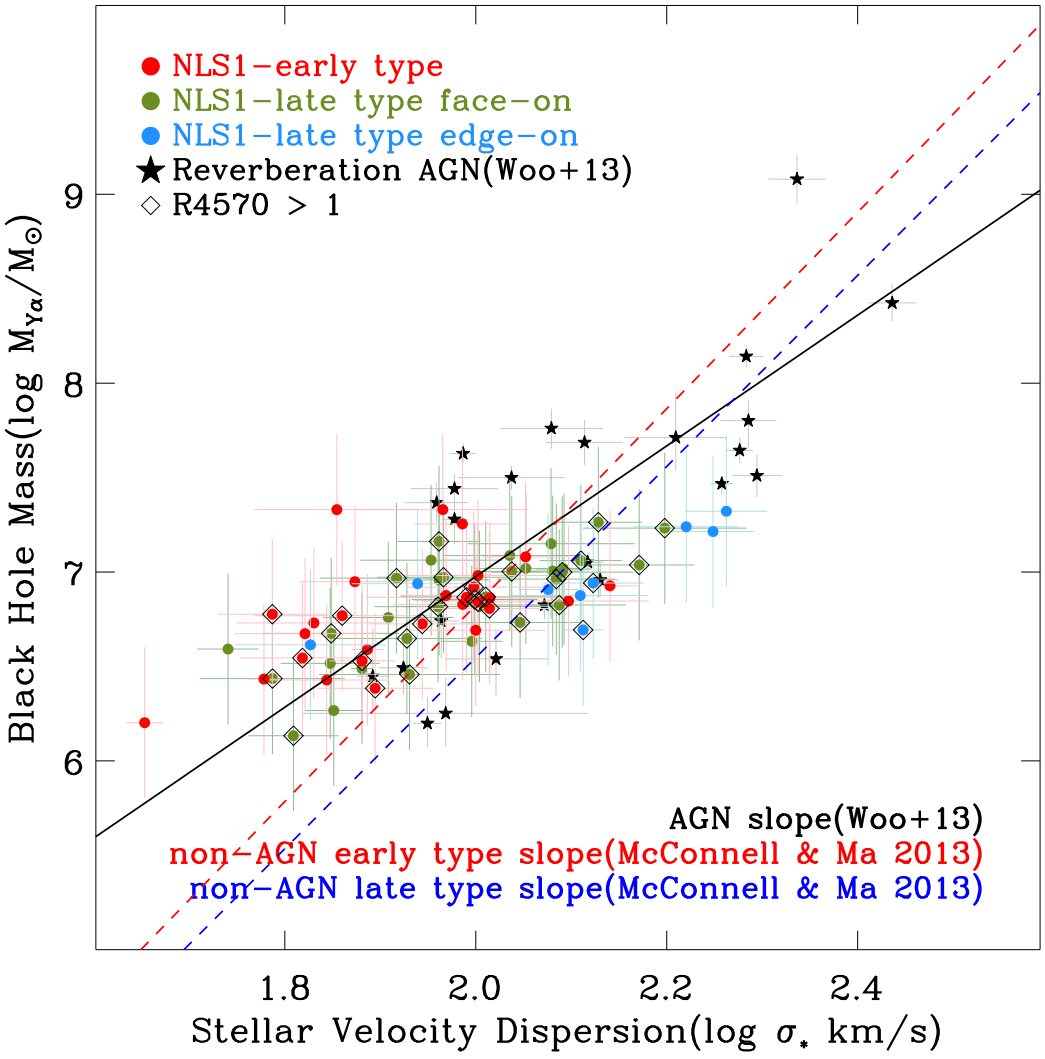

Figure 4.1: $M_{\rm BH} - \sigma_*$ of the NLS1s with early type (red circle), late type face-on (green circle) and late type edge-on galaxies (blue circle). The black hole mass is determined by equation 3.5 based on Hα measurements and the σ_* is measured in Mg b region with Mg b triplet. A sample of 25 reverberation−mapped AGNs from Woo et al. (2013) and its line fit are expressed in the black stars and the black solid line ($\alpha = 7.31$, $\beta = 3.46$). The results of line fit for 72 normal galaxies from McConnell & Ma (2013) are shown by two slopes, which are red dotted line for early type galaxies ($\alpha = 8.39$, $\beta = 5.20$) and blue dotted line for late type galaxies ($\alpha = 8.07$, $\beta = 5.06$). Additionally, black diamond symbols are used to show typical NLS1s emitting Fe II strongly with R4570 > 1.

The NLS1s seem to follow the AGN slope overall especially the early type and late type face-on galaxies. The offset of total sample from the AGN slope is -0.06 ± 0.04 dex, and it is 0.07 ± 0.06 dex for early type NLS1s, -0.09 ± 0.04 dex for late type face-on NLS1s. The edge-on NLS1s from the AGN slope, on the other hand, show somewhat larger offset from the AGN slope by -0.36 ± 0.11 dex. The negative offset of the edge-on NLS1s from the AGN slope can be explained by the rotation effect described in section 3.4. For the slopes determined based on normal galaxies from McConnell & Ma (2013), early type NLS1s show 0.35 ± 0.09 dex offset from the normal galaxy slope of the early types, and late type NLS1s including both edge-on and face-on NLS1s offset from the normal galaxy slope of the late types by 0.26 ± 0.07 dex. As a result, we found that the NLS1s have a trend to follow the $M_{\rm BH} - \sigma_*$ relation of AGN when the rotation effect is corrected for while the NLS1s lie above the $M_{\rm BH} - \sigma_*$ relations of normal galaxies with $\sim$0.3 dex offset.

To investigate one of the strongest features of NLS1s, strong Fe II, we divided our NLS1s into strong and weak Fe II emitters based on the criterion R4570 = 1 and compared them. The strong Fe II emitters with R4570 $>$ 1 show larger offset -0.11 ± 0.05 dex than the weak Fe II emitters having -0.02 ± 0.05 dex offset. Besides, the difference of $L/L_{\rm Edd}$ between these two groups is insignificant as only 0.02. As a result, the strong Fe II emitters tend to have larger offset and higher $L/L_{\rm Edd}$ than the weak Fe II emitters, however the difference is too minor to conclude that the $M_{\rm BH} - \sigma_*$ relation of NLS1s depends on Fe II strength.

To investigate systematic trend, we investigate a relation between the offset from the $M_{\rm BH} - \sigma_*$ relation and Eddington ratio as shown in Figure 4.2, but no correlation is found between them.

4.2 Comparison between σ_* and narrow emission line widths

The widths of [O III] λ5007 and [S II] $\lambda\lambda$6716, 6731 have been used commonly as a surrogate for stellar velocity dispersion by the difficulty of deriving σ_* as described in Chapter 1 (Mathur et al. 2001; Wang & Lu 2001; Botte et al. 2004; Grupe & Mathur 2004; Mathur & Grupe 2005a,b; Bian et al. 2006; Zhou et al. 2006; Komossa & Xu 2007; Watson et al. 2007). To investigate the reliability of using the narrow line width for σ_*, we compared the σ_* with the narrow line width of [O III] and [S II] in Figure 4.3. The widths lower than the spectral resolution could have uncertainty, thus those are not reliable to use. We will mainly discuss with the results with wider widths than the SDSS spectral resolution. First, the width of [S II] has -0.000 ± 0.016 dex mean offset with 0.131 dex rms scatter. There is no systematic offset, however there are a few targets having larger $\sigma_{[\mathrm{SII}]}$ measurements than the directly measured σ_*. These targets have low S/N of [S II], therefore the differences could be caused by the low quality of spectra. When the low quality targets are excluded, the $\sigma_{[\mathrm{SII}]}$ shows a good correlation with the σ_*. Meanwhile, in case of the width of [O III] core, the offset is 0.062 ± 0.022 dex and the rms scatter is 0.148 dex. The scatter is larger than its of the $\sigma_{[\mathrm{SII}]}$ case, and the distribution is widely scattered and no systematic trend is found. These results indicate the width of [O III] core has a very weak correlation with σ_*.

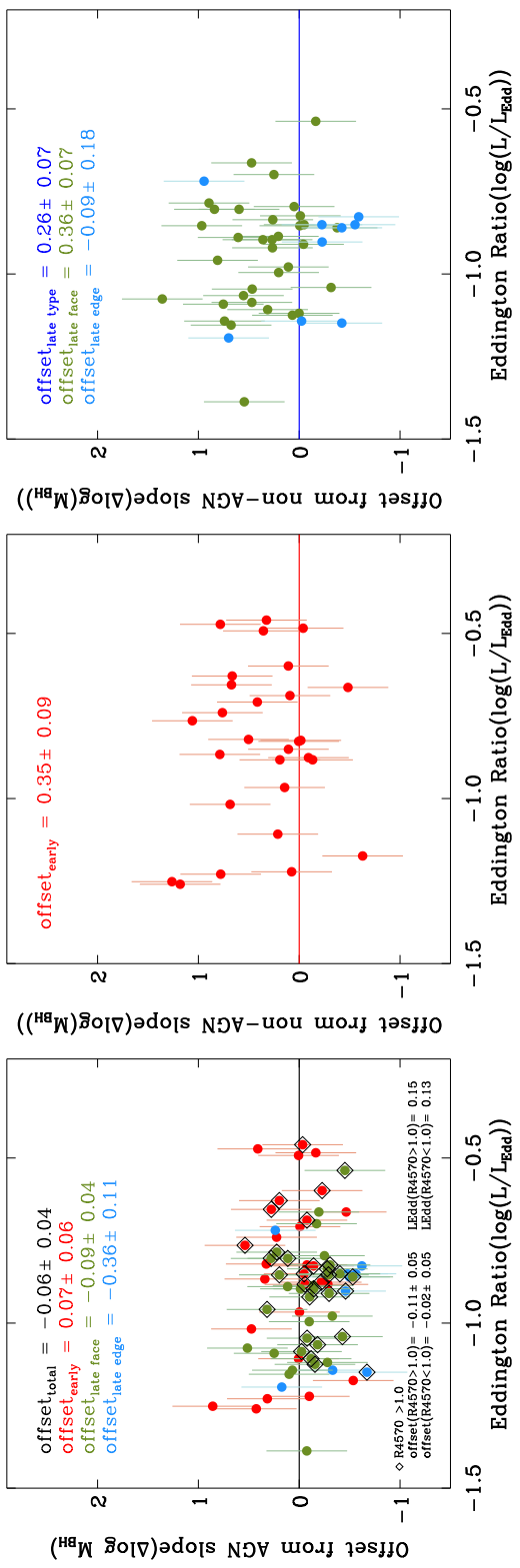

Figure 4.2: Relation between offset from the $M_{\rm BH} - \sigma_*$ relation and Eddington ratio for the NLS1s. From left to right figure, the y-axis represents the offset from the slope of reverberation−mapped AGNs from Woo et al. (2013), early type galaxies, and late type galaxies from McConnell & Ma (2013). The late type face-on and edge-on NLS1s are presented by green circles and blue circles, respectively, and the early type NLS1s are shown by red circles. As in Figure 4.1, NLS1s with R4570 > 1 is represented by black diamond additionally.

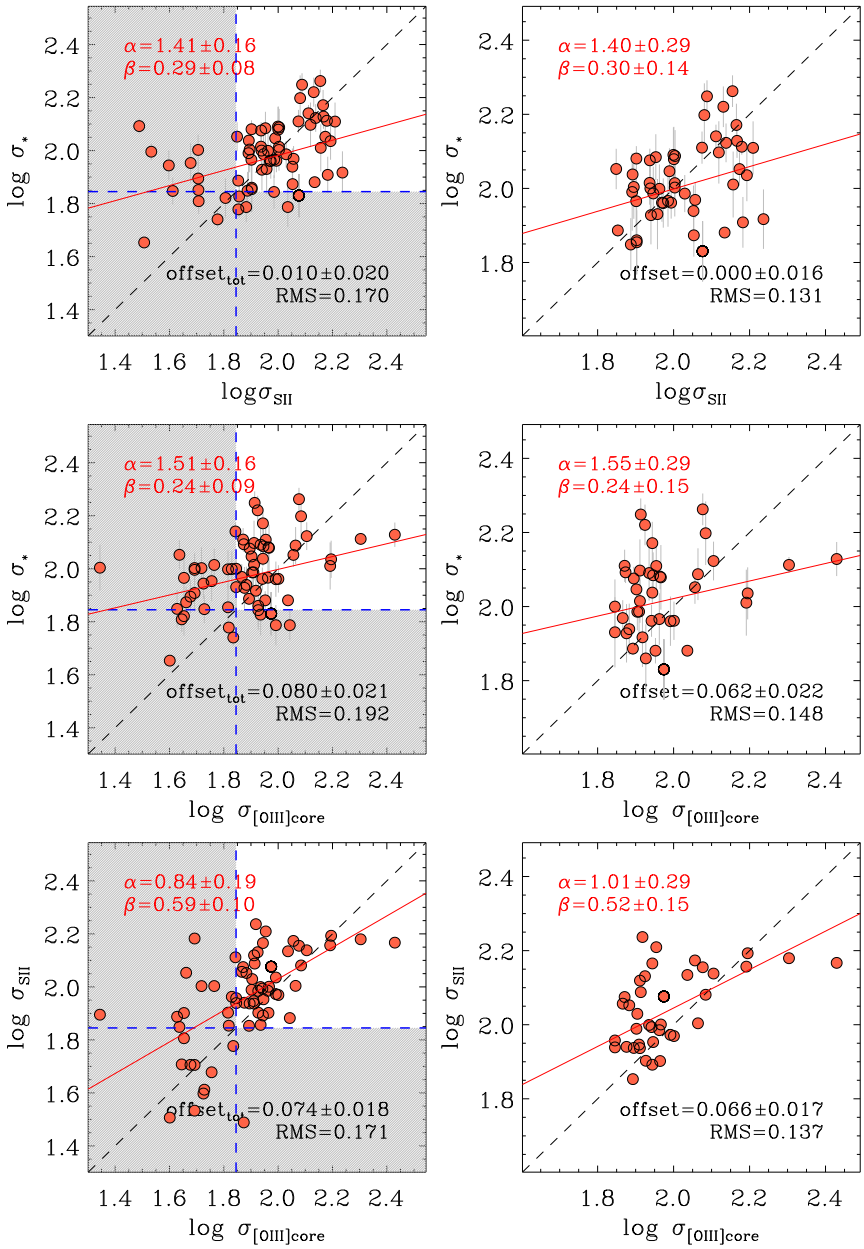

Figure 4.3: Comparisons of σ_* with $\sigma_{[\mathrm{OIII}]_{\mathrm{core}}}$ and $\sigma_{[\mathrm{SII}]}$. The [O III] is modeled by double Gaussian and measured the width of narrow core after excluding broad base component while the [S II] is fitted with a single Gaussian profile. The best-fit line showing trend between results is plotted by red solid line. In the figures in left column, the lower width region than the SDSS spectral resolution 70 km s^{-1} is expressed by gray shadow. The figures in right column show the targets having higher width than the spectral resolution only.

Chapter 5

Discussion

Previous observational studies have interpreted NLS1 galaxies are AGNs having low mass black holes typically accreting close to Eddington limit, thus NLS1s are believed to be young phase of AGNs (Véron-Cetty et al. 2001; Boroson 2002). Mathur et al. (2001) emphasized the importance of studying the $M_{\rm BH} - \sigma_*$ relation of NLS1s as a clue to understand the black hole growth and evolution and AGN feeding and feedback in galaxy evolution process. We therefore have homogeneously analyzed a sample of 71 NLS1 galaxies with the spectra of the SDSS DR7.

Location of the NLS1s on the $M_{\rm BH} - \sigma_*$ relation We present the $M_{\rm BH} - \sigma_*$ relation of the NLS1s in Figure 4.1 with results of RM AGNs and normal galaxies by dividing the NLS1s into three types: early type, late type face-on, and late type edge-on NLS1s. Note that the mass of black hole is calculated by equation 3.5 and the σ_* is measured in the Mg b region including Mg b triplet lines. Interestingly, the NLS1s seem to follow the $M_{\rm BH} - \sigma_*$ relation of AGNs when the edge-on NLS1s which are considered their σ_* are affected by the galactic rotation effect are excluded. Although there is the systematic uncertainty of the $M_{\rm BH}$ depending on the different methods, thus the uncertainty could be acceptable. Nevertheless, this issue would be one of the limitations in our study and more detailed investigation is needed. We suggest two possibilities for

this result: (1) the NLS1 galaxies are a prior stage of becoming BL AGNs, i.e., the NLS1s are evolving into BLS1 galaxies by tracking along the $M_{\rm BH} - \sigma_*$ relation. In this scenario, the $M_{\rm BH}$ should be grow by averagely a factor of 10 to evolve into BLS1s phase and it would take 10^8 years to reach assuming $L/L_{\rm Edd}$= 1.0. To maintain the $M_{\rm BH} - \sigma_*$ relation even after the black hole growth, the growth of σ_* corresponding to the $M_{\rm BH}$ growth should follow. Krongold et al. (2001) studied the growth of the host galaxy of NLS1s and indicated that there is no difference between the environments of Seyfert 1 and NLS1 galaxies, and Ryan et al. (2007) found that NLS1s are not preferentially merging system. Crenshaw et al. (2003); Ohta et al. (2007), however, indicated NLS1s show higher fraction of bar existence than BLS1s. In this case, a merger-induced black hole fueling or bar-induced fueling could be that solution to adjust the bulge properties. In other words, the black hole and the host galaxy of NLS1s will grow by affecting each other by AGN feeding and feedback in this scenario. The other possibility (2) is that NLS1s do not evolve into the BL AGNs, i.e., NLS1 galaxies are similar to other AGNs and NLS1s are simply the low mass extension of the BLS1s on the $M_{\rm BH} - \sigma_*$ relation as reported by McHardy et al. (2006). In this assumption, the high $L/L_{\rm Edd}$ of NLS1s could be explained by relatively short-lived accretion event to make only the black hole grow insignificantly, while the NLS1s having relatively low $L/L_{\rm Edd}$ would be before or after phase of the accretion event.

Rotation effect according to morphology A rotating disk of galaxy could bias the stellar velocity dispersions to higher values and cause a systematic offset. The rotating disk is more frequently shown in late types than in early types, and more edge-on galaxies more suffer from the rotation effect. To derive reliable σ_*, we classified NLS1s according to their morphology classifications. As expected, the late type edge-on galaxies show higher offset from the AGN slope and normal galaxy slopes than the other early type and late type fece-on galaxies. Excluding the late type edge-on NLS1s which are affected by the rotation effect, the rest NLS1s are seen on the slope of the

AGNs. To obtain more reliable σ_* and to correct the rotation effect, further studies are needed to confirm how the rotation of the disk influences to the σ_* measurements.

Narrow line widths as a surrogate for σ_* To test the reliability of using narrow line widths as a substitute for stellar velocity dispersion, we compared the directly measured σ_* with the widths of the core of [O III] λ5007 ($\sigma_{[\mathrm{OIII}]_{\mathrm{core}}}$) and [S II] $\lambda\lambda$6716, 6731($\sigma_{[\mathrm{SII}]}$) as illustrated in Figure 4.3. As a result, the width of [S II]($\sigma_{[\mathrm{SII}]}$), correlates with the σ_* while the width of [O III] ($\sigma_{[\mathrm{OIII}]_{\mathrm{core}}}$) does not, i.e., only $\sigma_{[\mathrm{SII}]}$ could be a reliable replacement of σ_*. The different ionization energy levels between [S II] and [O III]emissions would be the reason for this result. The [S II] has much lower ionization level (23.3 eV) than its of [O III] (54.9 eV), thus the location of the [O III] is closer to the black hole than its of the [S II]. Therefore the [O III] can be strongly influenced by the black hole activities, especially AGN outflow which is a strong wind made by the accretion of the black hole, and the [S II] could be more stable than the [O III].

Chapter 6

Summary & Conclusion

In this study, to investigate the connection between the black hole and the host galaxy of NLS1, we defined 433 NLS1s from the SDSS DR7 spectra (Abazajian et al. 2009) at relatively low redshift z $<$ 0.1. Two conventional definitions of NLS1s were used to define the NLS1s: (1) the FWHM of broad component of the Balmer lines ranges between 800 km s^{-1} and 2200 km s^{-1}, and (2) the line flux ratio between [O III] λ5007 and Hβ total emission lines (R5007) is less than 3 (Osterbrock & Pogge 1985; Goodrich 1989). The first criterion defines *narrow line* of NLS1 and the second criterion showing the line flux ratio of narrow line to broad line defines $seyfert$ 1 of NLS1. For the width condition, in order to include NLS1s positioning at the end of the characteristic, we used a definition having 200 km s^{-1} wider width range than well-known definition defined as 1000$-$2000 km s^{-1} (Osterbrock & Pogge 1985), however the other additional features, e.g., R5007, R4570, were used to characterize the NLS1s, using the definition of somewhat wider range could be a proper method to find NLS1s maximally. After defining the NLS1s, we measured the black hole mass by using Hα measurements due to the weakness of Hβ for our NLS1s. We calculated the $M_{\rm BH}$ from the virial relation by combining with the size$-$luminosity relation (Bentz et al. 2013) and the width relation between Hα and Hβ (Greene & Ho 2005). To compare the $M_{\rm BH}$ measurements, we

also measured the $M_{\rm BH}$ with the estimators from McGill et al. (2008), Greene & Ho (2005), and Park et al. (2012). For the stellar velocity dispersion, we measured σ_* for 71 NLS1s showing strong stellar spectrum enough to measure σ_*. In order to obtain more reliable measurements of σ_*, we measured the σ_* in three ways, $\sigma_{\rm Mgb}$, $\sigma_{\rm noMgb}$, and $\sigma_{\rm CaT}$, and compared each measurement. In addition, to consider the rotation effect on the σ_*, we classified 71 NLS1s according to their morphology types into early type, late type face-on, and late type edge-on galaxies.

As a result, we found that the NLS1s lie on the $M_{\rm BH} - \sigma_*$ relation of the AGNs excepting edge-on galaxies having relatively higher σ_* by the rotation effect. In other words, the NLS1 galaxies which are considered as young AGNs follow the $M_{\rm BH} - \sigma_*$ relation of the AGNs as BL AGNs if we exclude the rotation effect of galactic disk. With this result, we suggest two possibilities as follows. The first is NLS1s are on a prior stage of BLS1s and are evolving into BLS1s along the $M_{\rm BH} - \sigma_*$ relation. If NLS1 galaxies follow this scenario, NLS1s should maintain high accretion rate sustainedly and the host galaxy of NLS1s also has to grow along with the black hole growth. This could be explained by AGN feeding and feedback between black hole and host galaxy, e.g., merger-induced or bar-induced gas fueling into black hole, AGN outflow. The second possibility is that NLS1s are not unusual AGNs and simple seyfert 1 galaxies positioning near the low mass end of the $M_{\rm BH} - \sigma_*$ relation. In other words, NLS1 galaxies do not evolve into BLS1s and the high $L/L_{\rm Edd}$ of NLS1s is considered as just very short accretion event affecting marginally.

Furthermore, we checked reliability of using the narrow line widths, $\sigma_{\rm [OIII]_{core}}$, $\sigma_{\rm [SII]}$, as a surrogate for σ_*. In our results, a good correlation is found between σ_* and $\sigma_{\rm [SII]}$while $\sigma_{\rm [OIII]_{core}}$ shows very weak correlation to σ_* and large scatter. This different results between [S II] and [O III] could be interpreted by the difference of ionization energy levels of narrow lines. The [S II] has much lower ionization level than [O III] therefore [S II] would be much less influenced by the black hole activity hence [S II] gas

could be more stable state. Therefore we conclude $\sigma_{[\mathrm{SII}]}$ could be a good replacement of σ_* while $\sigma_{[\mathrm{OIII}]_{\mathrm{core}}}$ is unreliable on account of a weak correlation with the σ_* in large scatter.

Bibliography

Abazajian, K. N., Adelman-McCarthy, J. K., Agüeros, M. A., et al. 2009, ApJS, 182, 543

Antonucci, R. 1993, ARA&A, 31, 473

Barth, A. J., Ho, L. C., & Sargent, W. L. W. 2002, ApJ, 566, L13

—. 2003, ApJ, 583, 134

Bennert, V. N., Auger, M. W., Treu, T., Woo, J.-H., & Malkan, M. A. 2011, ApJ, 726, 59

Bentz, M. C., Peterson, B. M., Netzer, H., Pogge, R. W., & Vestergaard, M. 2009a, ApJ, 697, 160

—. 2009b, ApJ, 697, 160

Bentz, M. C., Denney, K. D., Grier, C. J., et al. 2013, ApJ, 767, 149

Bian, W., Yuan, Q., & Zhao, Y. 2006, MNRAS, 367, 860

Boroson, T. A. 2002, ApJ, 565, 78

Boroson, T. A., & Green, R. F. 1992, ApJS, 80, 109

Botte, V., Ciroi, S., Rafanelli, P., & Di Mille, F. 2004, AJ, 127, 3168

Bruzual, G., & Charlot, S. 2003, MNRAS, 344, 1000

Crenshaw, D. M., Kraemer, S. B., & Gabel, J. R. 2003, AJ, 126, 1690

Ferrarese, L., & Merritt, D. 2000, ApJ, 539, L9

Gebhardt, K., Bender, R., Bower, G., et al. 2000, ApJ, 539, L13

Goodrich, R. W. 1989, ApJ, 342, 224

Greene, J. E., & Ho, L. C. 2005, ApJ, 630, 122

Grupe, D. 2004, AJ, 127, 1799

Grupe, D., & Mathur, S. 2004, ApJ, 606, L41

Häring, N., & Rix, H.-W. 2004, ApJ, 604, L89

Harris, C. E., Bennert, V. N., Auger, M. W., et al. 2012, ApJS, 201, 29

Kang, W.-R., Woo, J.-H., Schulze, A., et al. 2013, ApJ, 767, 26

Kaspi, S., Maoz, D., Netzer, H., et al. 2005, ApJ, 629, 61

Kaspi, S., Smith, P. S., Netzer, H., et al. 2000, ApJ, 533, 631

Komossa, S., & Xu, D. 2007, ApJ, 667, L33

Komossa, S., Xu, D., Zhou, H., Storchi-Bergmann, T., & Binette, L. 2008, ApJ, 680, 926

Krongold, Y., Dultzin-Hacyan, D., & Marziani, P. 2001, AJ, 121, 702

Lawrence, A., Saunders, W., Rowan-Robinson, M., et al. 1988, MNRAS, 235, 261

Leighly, K. M. 1999, ApJS, 125, 317

Marconi, A., & Hunt, L. K. 2003, ApJ, 589, L21

Markwardt, C. B. 2009, in Astronomical Society of the Pacific Conference Series, Vol. 411, Astronomical Data Analysis Software and Systems XVIII, ed. D. A. Bohlender, D. Durand, & P. Dowler, 251

Mathur, S., & Grupe, D. 2005a, A&A, 432, 463

—. 2005b, ApJ, 633, 688

Mathur, S., Kuraszkiewicz, J., & Czerny, B. 2001, New A, 6, 321

McConnell, N. J., & Ma, C.-P. 2013, ApJ, 764, 184

McGill, K. L., Woo, J.-H., Treu, T., & Malkan, M. A. 2008, ApJ, 673, 703

McHardy, I. M., Koerding, E., Knigge, C., Uttley, P., & Fender, R. P. 2006, Nature, 444, 730

Merritt, D., & Ferrarese, L. 2001, ApJ, 547, 140

Nelson, C. H. 2000, ApJ, 544, L91

Nelson, C. H., Green, R. F., Bower, G., Gebhardt, K., & Weistrop, D. 2004, ApJ, 615, 652

Ohta, K., Aoki, K., Kawaguchi, T., & Kiuchi, G. 2007, ApJS, 169, 1

Onken, C. A., Ferrarese, L., Merritt, D., et al. 2004, ApJ, 615, 645

Osterbrock, D. E. 1978, Proceedings of the National Academy of Science, 75, 540

Osterbrock, D. E., & Pogge, R. W. 1985, ApJ, 297, 166

Park, D., Woo, J.-H., Treu, T., et al. 2012, ApJ, 747, 30

Peterson, B. M., Ferrarese, L., Gilbert, K. M., et al. 2004, ApJ, 613, 682

Ryan, C. J., De Robertis, M. M., Virani, S., Laor, A., & Dawson, P. C. 2007, ApJ, 654, 799

Valdes, F., Gupta, R., Rose, J. A., Singh, H. P., & Bell, D. J. 2004, ApJS, 152, 251

van der Marel, R. P. 1994, MNRAS, 270, 271

Vanden Berk, D. E., Richards, G. T., Bauer, A., et al. 2001, AJ, 122, 549

Véron-Cetty, M.-P., Véron, P., & Gonçalves, A. C. 2001, A&A, 372, 730

Wang, T., & Lu, Y. 2001, A&A, 377, 52

Watson, L. C., Martini, P., Dasyra, K. M., et al. 2008, ApJ, 682, L21

Watson, L. C., Mathur, S., & Grupe, D. 2007, AJ, 133, 2435

Williams, R. J., Pogge, R. W., & Mathur, S. 2002, AJ, 124, 3042

Woo, J.-H., Treu, T., Malkan, M. A., & Blandford, R. D. 2006, ApJ, 645, 900

Woo, J.-H., & Urry, C. M. 2002, ApJ, 579, 530

Woo, J.-H., Urry, C. M., Lira, P., van der Marel, R. P., & Maza, J. 2004, ApJ, 617, 903

Woo, J.-H., Urry, C. M., van der Marel, R. P., Lira, P., & Maza, J. 2005, ApJ, 631, 762

Woo, J.-H., Treu, T., Barth, A. J., et al. 2010, ApJ, 716, 269

Xiao, T., Barth, A. J., Greene, J. E., et al. 2011, ApJ, 739, 28

Xu, D., Komossa, S., Zhou, H., et al. 2012, AJ, 143, 83

Zhou, H., Wang, T., Yuan, W., et al. 2006, ApJS, 166, 128

초 록

우리는 Sloan Digital Sky Survery DR7 (SDSS DR7) 을 사용하여 좁은 방출선폭 세이퍼트 1 은하 (Narrow Line Seyfert 1 Galaxies 또는 NLS1) 의 블랙홀 질량과 모은하의 별속도분산과의 상관관계에 대해서 연구를 진행하였다. 좁은 방출선폭 세이퍼트 1 은하는 상대적으로 좁은 발머 방출선을 보이는 은하를 말한다. 이 은하들은 대체적으로 낮은 블랙홀 질량을 가지면서 동시에 높은 에딩턴 비율을 갖는 아주 특이한 현상을 보인다. 이로 인해 블랙홀 질량과 모은하의 간의 상관관계 및 공동진화 연구에 중요한 단서를 제공할 것이라고 여겨져 최근까지 NLS1 은하에 대한 많은 연구가 진행되었다. 현재까지의 연구에서는 밝은 활동성 은하핵과 강한 Fe II 방출선의 영향으로 은하의 별속도분산을 직접 측정하기가 어려워, 별속도분산과 좁은 선폭 방출선의 속도분산과의 상관관계가 밝혀진 이후로 많은 연구에서 [O III] λ5007, [S II] $\lambda\lambda$6716, 6731, [N II] $\lambda\lambda$6548, 6583 방출선들의 속도분산값을 별속도분산의 대체값으로 사용하였다. 하지만 이 방출선들을 어떻게 측정하느냐에 따라서, 또 어떤 표본을 사용하느냐에 따라서 그 결과가 많이 달라져 이 방법에 대한 신뢰는 계속해서 논의되고 있는 상황이다. 우리는 이 연구에서 은하의 별속도분산을 직접 측정하여 좁은 방출선폭 세이퍼트 1 은하의 블랙홀과 은하 상관관계에 대해서 연구하였고, 나아가 좁은 선폭 방출선들의 별속도분산의 대체값으로서의 사용가능성에 대해서도 확인하였다. 그 결과, 좁은 방출선폭 세이퍼트 1 은하들도 다른 활동은하에서 보이는 $M_{\rm BH} - \sigma_*$ 상관관계를 따름을 확인하였고, 좁은 선폭 방출선들 중 [S II] 의 경우, 직접 측정한 별속도분산과 상관관계를 보여 별속도분산의 대체값으로 사용가능하다는 결론을 내렸다.

주제어: 은하: 활동성 은하핵 – 퀘이사: 방출선

Student Number: 2011 − 23286